

# Stable isotope study of the mineralization and alteration in the Madjarovo Pb–Zn district, south-east Bulgaria

Clive M. Rice · Richard J. McCoyd · Adrian J. Boyce · Peter Marchev

Received: 23 March 2005 / Accepted: 12 February 2007 / Published online: 10 March 2007  
© Springer-Verlag 2007

**Abstract** The Madjarovo ore district is centred on the exposed section of a Lower Oligocene volcano and consists of radially disposed Pb–Zn-precious metal veins and attendant intermediate sulfidation wallrock alteration. Earlier high sulfidation and potassic porphyry style alterations are found in the centre of the district spatially associated with monzonitic intrusions. The total duration of all mineralization and alteration was ca. 300 ka. Stable isotope analyses (S, O, H) have been carried out on a suite of sulfides, sulfates and silicates from the mineralization, high and intermediate sulfidation alterations and a suite of basement rocks. These data range between the following limits:  $\delta^{34}S_{\text{sulfides}} = -1.2$  to  $+6.8\text{‰}$ ;  $\delta^{34}S_{\text{sulfates}} = +21.4$  to  $+24.9\text{‰}$ ;  $\delta^{18}O_{\text{sulfates}} = +5.8$  to  $+11.6\text{‰}$ ;  $\delta D_{\text{sulfates}} = -35.1$  to  $-67.1\text{‰}$ ;  $\delta^{18}O_{\text{silicates}} = +5.2$  to  $+13.5\text{‰}$ ;  $\delta D_{\text{silicates}} = -36.3$  to  $-77.0\text{‰}$ . We also analysed  $\delta D$  of fluid inclusions in quartz and barite for which we obtained, respectively, the ranges of  $-43.6$  to  $-78.6$  and  $-58.4$  to  $-67.1\text{‰}$ . The data show that high sulfidation alteration was dominated by magmatic fluids with minor meteoric water, whereas the fluids responsible for the intermediate sulfidation alteration were essentially magmatic. The fluids responsible for

the intermediate sulfidation Pb–Zn mineralization were mixed magmatic–meteoric and certainly contained a significant meteoric component. Sulphur is likely derived from basement and/or igneous sources. The evolution of alteration and mineralization styles from potassic, porphyry copper style to high sulfidation to intermediate sulfidation can be understood in terms of changing ore fluid composition resulting from an increasing permeability of the system and an increasingly remote source of magmatic fluid with time. These changes link directly to the geological evolution of this volcanic centre.

**Keywords** Stable isotopes · Pb–Zn mineralization · Alteration · Madjarovo · Bulgaria

## Introduction

The Madjarovo Pb–Zn-precious metal mining district is located within the Rhodope Massif in southeastern Bulgaria, approximately 200 km southeast of Sofia (Fig. 1). The deposit is a part of the Rhodope metallogenic province (Stoyanov 1979) that comprises numerous volcanic- and sediment-hosted epithermal deposits, and metamorphic basement-hosted hydrothermal base-metal vein and replacement deposits (Marchev et al. 2000, 2005). The mineralization is hosted by an Early Oligocene volcanic centre and comprises Pb–Zn and precious metal mineralization with associated potassic-(porphyry) style and epithermal style (high and intermediate sulfidation) alteration within a very restricted area (Marchev et al. 1997, 2005). Recent field observations and  $^{40}\text{Ar}/^{39}\text{Ar}$  data (Marchev et al. 1997; Marchev and Singer 2002) have suggested close relationships between alteration and rock-type potassic, and barren high sulfidation alteration are associated with monzonitic stocks, whereas younger trachytic dykes are associated with

Editorial handling: S. Nicolescu

C. M. Rice (✉) · R. J. McCoyd  
Department of Geology and Petroleum Geology,  
University of Aberdeen,  
Aberdeen AB24, Scotland, UK  
e-mail: c.rice@abdn.ac.uk

A. J. Boyce  
Scottish Universities Research and Reactor Centre,  
East Kilbride, Glasgow,  
Scotland G75 0QU, UK

P. Marchev  
Geological Institute, Bulgarian Academy of Sciences,  
Sofia 1113, Bulgaria

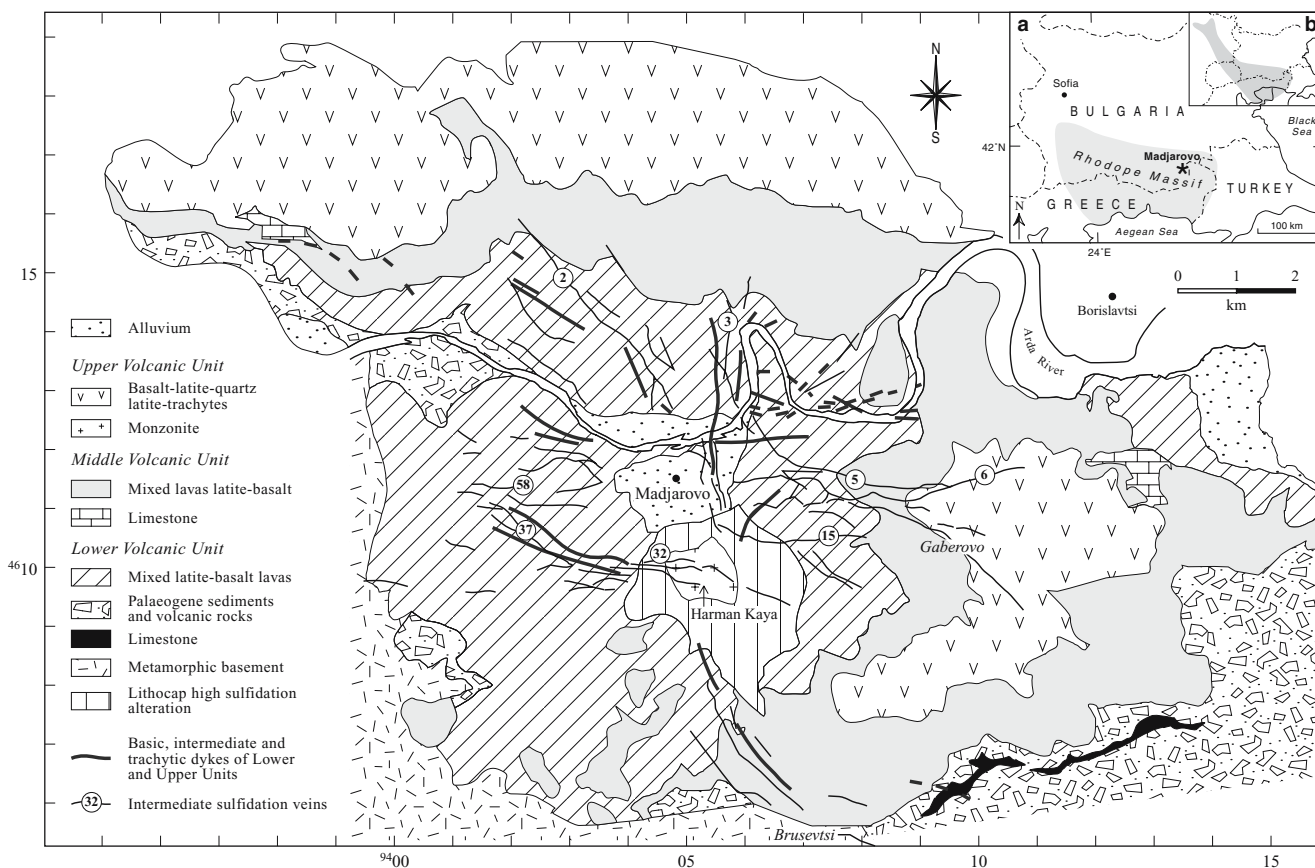


**Fig. 1** Geologic map of the Madjarovo volcano and ore district (modified from Marchev and Singer 2002). Sampled veins are numbered or named. *Inset A* Location of the Rhodope Massif and of

the Madjarovo ore district. *Inset B* The extent of the Paleogene Macedonian–Rhodope–North–Aegean Magmatic arc. Co-ordinates refer to the international grid system

intermediate sulfidation alteration. The role of magmas in the formation of the Madjarovo mineralization is supported by galena Pb isotope data (Marchev et al. 2005 and references therein), which demonstrate overall similarity between the initial isotopic composition of galena and K-feldspars from the magmatic rocks.

This paper presents the results of a stable isotope study (S, O, H) on the intermediate-sulfidation alteration and related Pb–Zn-precious metal mineralization and also the barren high sulfidation alteration, providing further insights into the genesis of this complex magmatic-hydrothermal system. The main objectives of the study are (1) to identify the sources of S in the Madjarovo system, (2) to characterise and identify the sources of the fluids responsible for the above-mentioned mineralization and alteration and (3) to build on the previous studies of Madjarovo to produce an integrated model of the Madjarovo magmatic and hydrothermal system.

### Mining and exploration history

Mining at Madjarovo is believed to have commenced during Thracian times (~2,500 BP), but the vast majority of the development dates from economic expansion during the early

days of the soviet-backed government in the mid-twentieth century. Overall, about 10.8 Mt of ore grading ~1.3% Pb and 0.7% Zn were processed from the Madjarovo district (Milev et al. 1996). Another 6.5 Mt of base metal reserves and large amounts of low-grade ore remain. About 0.3 Mt of gold at 2–3 g/t were extracted from the upper parts of two of the base metal veins. Because of changes in the Bulgarian economy and a decrease of ore grade with depth, mining operations are now uneconomic and have been stopped. An extensive gold exploration program was performed between 1988 and 1996 by the Jambol exploration organisation in the upper parts of the base metal veins. Eight to 9 major veins have been explored so far, and the proven reserves are about 2 million metric tons, grading 3.9 g/t Au. However, a feasibility study completed in 1995 by Eurast indicated that the ore deposit is not economically viable.

### Regional geologic setting

The Rhodope massif, located in southern Bulgaria and northern Greece, is regarded as the most internal zone of the Alpine–Himalayan orogenic system in the eastern Mediterranean region (inset A, Fig. 1). The massif is an

east-west-oriented complex underlain by a high-grade, mainly amphibolite facies, metamorphic basement. Two major tectonostratigraphic units (complexes) have been recognised in the eastern part of the massif on the basis of metamorphic rock composition: a gneiss-migmatite complex and a variegated complex (Kozhoukharov et al. 1988; Haydoutov et al. 2001). The gneiss-migmatite complex is dominated by orthometamorphic rocks including metagranites, migmatites and migmatised gneisses and is overlain by metasediments. Eclogitic rocks have been described from the Greek side of the Rhodopes (Mposkos and Krohe 2000). The overlying variegated complex consists of a heterogeneous assemblage of metasedimentary rocks and ophiolite bodies intruded by metamorphosed intermediate to mafic rocks (Kozhoukharova 1984; Kolcheva and Eskenazy 1988). Recently obtained zircon U–Pb age data from different parts of the Rhodope massif clearly suggest that it experienced a complex and varied geologic history that is not completely understood. These ages show that the gneiss-migmatite complex is formed of Variscan or possibly Proterozoic continental basement (Peytcheva and von Quadt 1995; Carrigan et al. 2003). Late Neoproterozoic ages ( $572 \pm 5$  Ma) have also been obtained from the overlying variegated complex (Carrigan et al. 2003). The variegated complex is tectonically overlain by metasediments and mafic and ultra-mafic metaigneous rocks of Jurassic–Lower Cretaceous age, traditionally assigned to the Circum–Rhodope Belt (Jaranov 1960; Kockel et al. 1977).

In Alpine times the Rhodope Massif was characterised by a complicated tectono-metamorphic evolution. Ivanov (1989) and Burg et al. (1990) distinguish two phases in the evolution of the Rhodopes. The first phase, in the Mid-Cretaceous (110–90 Ma), caused large-scale compression with south-vergent thrusting and amphibolite-facies metamorphism. It was followed by two stages of extensional tectonics as the orogen collapsed beginning in the Upper Cretaceous–Paleogene time (Marchev et al. 2004). Initiation of extension is constrained by the formation of metamorphic core complexes, low-angle detachment faults and supra-detachment Maastrichtian–Paleocene sedimentary basins, intimately associated with 70–42 Ma granitoids and metamorphism. The later Eocene–Oligocene stage started with block faulting, sedimentary basin formation and extensive acid, intermediate and basic volcanism over the entire Rhodope area that led to the formation of the Macedonian–Rhodopian–North Aegean magmatic arc (Harkovska et al. 1989; Marchev and Shanov 1991; inset B, Fig. 1). The sedimentary basins and volcanism are fault-controlled with orientation changing across the region from NNW–SSE in the west to E–W in the Eastern Rhodopes (Kharkovska 1984; Jones et al. 1992). During this last extensional stage, a range of hydrothermal ore deposits, including Madjarovo, were formed in the Rhodopes (Marchev et al. 2005).

## District geology

The geology of the Madjarovo district has been summarised by Breskovska et al. (1976), Maznikov and Văleva (1986), Gergelchev (1974) and Marchev et al. (1997). It is dominated by volcanic rocks of Oligocene age, which cover an area of about 120 km<sup>2</sup> and reside within an east-west-trending sedimentary basin, also containing Eocene conglomerates, sandstones and coral limestones deposited under shallow marine conditions (Goranov and Atanasov 1989; Fig. 1). These Tertiary rocks rest upon the basement of the Rhodope Massif (see above).

The Arda River flows from west to east along the major Arda fault and dissects the central part of the volcanic sequence. The erosion here provides about 700 m of vertical relief and access to deep stratigraphic levels. Volcanic activity was of predominantly fissure type and formed a shield volcano (Ivanov 1960). The volcanics are dominated by large sheet-like lava flows and subordinate reworked volcanic fragmental rocks (epiclastics). The latest lava flows interfinger with coral reef limestones, indicating that the periphery of the volcano was submerged at least until the end of volcanism. The core of the volcano at this late stage was emergent and vegetated as evidenced by the presence of carbonised branches in the late epiclastics.

The volcanic lithologies comprise basic to intermediate rocks of shoshonitic to high-K calc-alkaline affinities with latites being the most voluminous rock type. The most acidic rocks are of quartz trachyte composition (Marchev et al. 1989). Based on the compositional and isotopic evolution (Sr and O), Marchev et al. (1994a, 2005) and Marchev and Rogers (1998) distinguished three units in the evolution of the volcano (Fig. 1). A summary of the evolution and timing of the magmatic and hydrothermal processes based on these studies is presented below and sketched in Fig. 2.

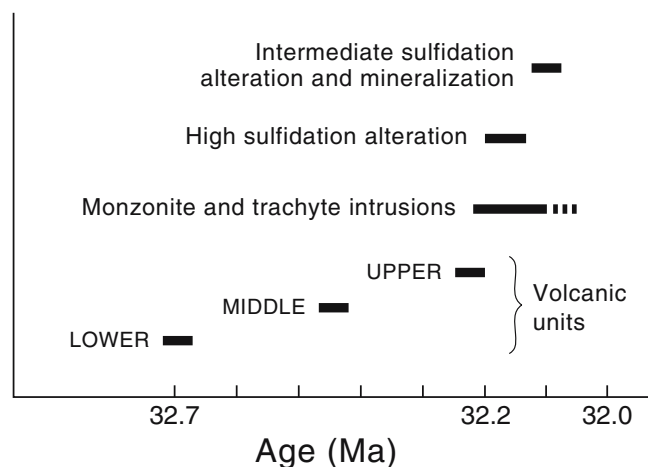


**Fig. 2** Timing of igneous and hydrothermal activity at Madjarovo (simplified after Marchev and Singer 2002)

**Lower and middle units** These two volcanic units began with the emplacement of a thick (up to 150 m) latite flow (Arda latite) and ended with basalts. Bracketed between them are thinner flows of basaltic andesites to andesites, showing petrographic and isotopic evidence for large-scale mingling and mixing processes between those end members (Marchev et al. 1994b). The lowermost latite flow was dated by  $^{40}\text{Ar}/^{39}\text{Ar}$  biotite total fusion in two samples, yielding ages of  $32.66 \pm 0.15$  and  $32.69 \pm 0.21$  Ma. A separate step-heating biotite spectrum of the second sample yielded a similar age of  $32.72 \pm 0.23$ . These ages are statistically indistinguishable from the age of the underlying Rezeda tuff ( $32.44 \pm 0.23$  Ma) composed of pumice and ash-fall tuff (Marchev and Singer 2002).

**Upper unit** This unit consists of several lava flows that cover the whole compositional range in the volcano from high-K, high-Al basalts to quartz-latite. The topmost quartz latite flow was dated by sanidine incremental heating and total-fusion, yielding  $^{40}\text{Ar}/^{39}\text{Ar}$  ages of  $32.23 \pm 0.19$  and  $32.16 \pm 0.18$  Ma, respectively (Marchev and Singer 2002), which are in excellent agreement with the  $32.3 \pm 0.6$  Ma age obtained by a clinopyroxene–plagioclase–biotite–sanidine Rb–Sr isochron by Marchev and Rogers (1998; Fig. 2).

**Intrusive rocks** Radial porphyritic dykes with compositions similar to the lava flows crop out in the central part of the volcanic structure, suggesting that they may have served as feeders (Fig. 1). The Lower Unit volcanic rocks are intruded by elongate or circular stocks of monzonite, monzogabbro and syenite that may coalesce at depth (Mavroudchiev 1959). Only the largest of these, Harman Kaya, is shown in Fig. 1. A gravity minimum and magnetic anomaly beneath the central part of the complex have been interpreted as generated by a syenitic pluton at a depth of between 1 and 4 km (Iosifov et al. 1987). The intrusion of monzonite–trachyte magma appears to have been preceded, accompanied and followed by the formation of radial fissures that were filled by dykes and finally hydrothermal veins. This intrusive phase was also responsible for the destruction of the central part of the volcano. Gergelchev (1974) postulated the existence of a caldera structure coinciding in size with the pluton, but the results of extensive drilling and our field observations do not confirm this interpretation. The largest monzonite body named “Harman Kaya” ( $\sim 1.5 \text{ km}^2$ ) and the trachytic dykes cutting the whole volcanic pile have identical composition. The monzonite and trachytes have similar Sr and Nd isotopic signatures to the volcanic rocks of the Upper Unit (Marchev et al. 2002), and their belonging to the latest magmatic event is confirmed by the age of a trachyte ( $32.06 \pm 0.13$  Ma; Marchev and Singer 2002; Fig. 2).

## Hydrothermal alteration

Previous studies of hydrothermal alteration at Madjarovo have been published by Radonova (1960), Breskovska et al. (1976), Velinov and Nokov (1991), McCoyd (1995, unpublished data) and Marchev et al. (1997). Alteration assemblages at Madjarovo may be classified as epithermal (high and intermediate sulfidation) and subjacent potassic porphyry style (Marchev et al. 1997, 2005). The spatial and temporal relationships between the various alteration assemblages, mineralization and evolutionary phases of the volcanic complex are shown in Figs. 2 and 3.

The emplacement of shallow-level monzonite stocks at the end of magmatic activity was accompanied by the development of either barren porphyry and/or high sulfidation styles of alteration. The former alteration is represented by hydrothermal biotite, K-feldspar, albite and contains disseminated pyrite with weak chalcopyrite mineralization. Epithermal alteration, which is of most interest in this paper, consists of five main alteration assemblages, which may be described as advanced-argillic, sericite, propylitic, quartz–sericite and adularia–sericite (McCoyd, 1995, unpublished data). The first two and last two were formed within high sulfidation and intermediate sulfidation environments, respectively (Sillitoe and Hedenquist 2003; Einaudi et al. 2003).

Propylitic alteration is generally weak but widely developed and is especially common in the central parts of the volcanic structure. Some propylitic alteration is pre-ore (Radonova 1960), associated with high sulfidation alteration and the formation of the lithocap (see below), whereas the rest is associated with the formation of intermediate sulfidation alteration and the base/precious metal veins. Chlorite, carbonate and epidote are the common alteration products.

High sulfidation alteration is developed around the largest outcrop (Harman Kaya) of the Madjarovo monzonite intrusion in the central portion of the palaeo-volcano (Fig. 1). It consists of kaolinite, pyrophyllite, alunite and diaspore (advanced argillic alteration) with alunite alteration occurring at the highest elevation. Vuggy silica is also present in the upper part of the intrusion but is not well developed and appears to form as irregular lenses. It grades outwards through sericite alteration, consisting predominantly of muscovite, quartz and pyrite and minor dickite to form a lithocap (Sillitoe et al. 1998). It is noteworthy that the acid sulfate alteration system is barren and not directly associated with base-metal mineralization.

Intermediate sulfidation quartz–sericite alteration is mainly associated with the deeper portions of the base metal veins but is also found at higher levels, associated with adularia–sericite alteration (see below). It is strongly fracture controlled and forms envelopes around quartz veins. Collectively, these linear alteration zones and

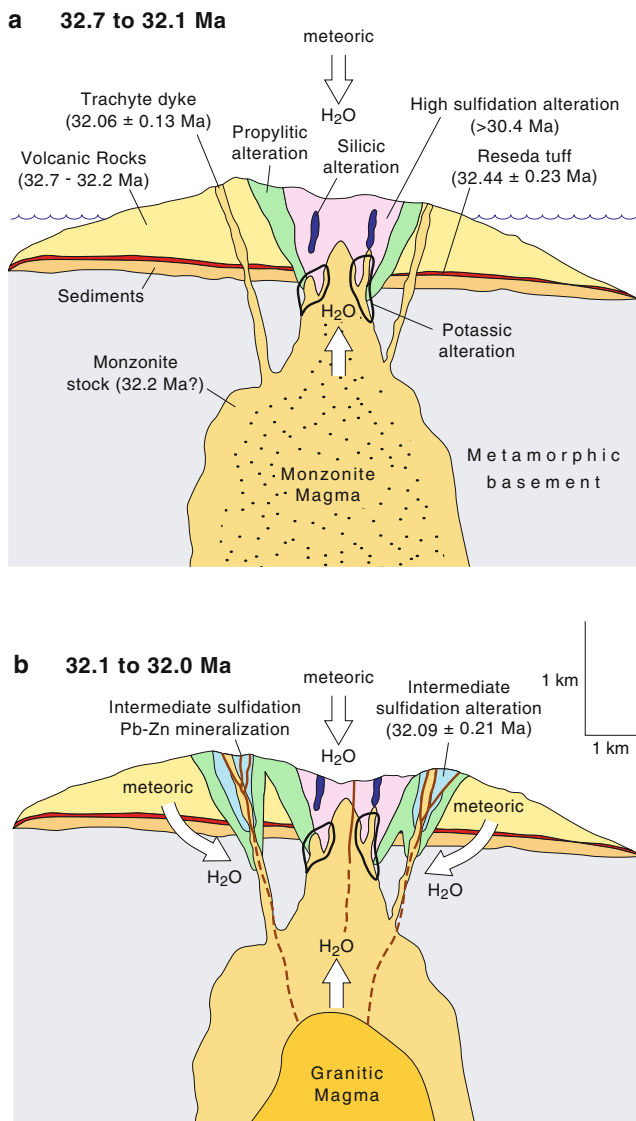


**Fig. 3** Two-stage evolution of the Madjarovo volcano showing the spatial and temporal relationships between the alteration assemblages, mineralization and igneous phases of the volcanic complex. **a** 32.7 to 32.1 Ma: growth of emergent shield volcano followed by uplift, erosion and formation of barren, high sulfidation lithocap. **b** 32.1 to 32.0 Ma: fresh injection of more differentiated magma, further uplift and erosion, opening of radial fissures and filling by intermediate sulfidation Pb–Zn mineralization (modified from Marchev and Singer 2002)

associated base-metal veins are developed radially and echo the stress field associated with dyke emplacement. Typically, the width of the zone is a few tens of centimetres but can be up to several meters around larger veins. Quartz and sericite are the main minerals but subordinate illite and smectite are also found together with disseminated pyrite. The sericite replaces feldspar and also occurs in the groundmass, whereas the quartz occurs as veinlets that become more common closer to the veins.

The adularia–sericite alteration is strongly associated with base-metal mineralization and is typically found in the upper levels of the palaeo-volcano and extends up to 120 m

on either side of these veins. In hand specimens, the rocks are light grey in colour but weather to a pale pink or pinkish brown. The most intensely altered rocks consist of a fine-grained aggregate of quartz and adularia only. Usually sericite is present and may reach up to 40%. Small quantities of aluminium–phosphate–sulfate minerals are also found. Cross-cutting relationships in the centre of the district indicate that intermediate sulfidation alteration postdates high sulfidation alteration.

Whereas the temperature range for the intermediate sulfidation alteration can be inferred from fluid inclusion studies of the base metal veins, we have no fluid inclusion data for the high sulfidation alteration stage. Instead, two methods were employed to estimate a formation temperature for the latter stage; these were stable isotope geothermometry and the thermal stabilities of the mineral phases present. The former technique used oxygen and sulphur isotope data from suitable minerals from the same outcrop. The mineral pairs used were alunite–pyrite and quartz–muscovite, and the temperatures obtained ranged from 280 to 347°C (McCoyd, 1995, unpublished data). The bottom end of the temperature range is in reasonable agreement with an estimate based on the mineral assemblage pyrophyllite, diaspore and zunyite, which indicates a formation temperature of 250°C or higher (Reyes 1990). The presence of a significant degree of replacement of alunite by woodhouseite and svanbergite at Madjarovo (McCoyd, 1995, unpublished data) also implies relatively high temperatures (Stoffregen and Alpers 1987). These calculations suggest that a formation temperature of 280–350°C is reasonable for the high sulfidation stage.

### Mineralization

The base metal and Au mineralization at Madjarovo is located in the central part of the volcano, spatially associated with trachyte dykes. The ore veins are hosted within a 700- to 800-m-thick volcanic pile and extend into the basement metamorphic rocks. Brusevtsi is the only deposit located outside the volcano and is hosted entirely within metamorphic rocks. Approximately 150 quartz–sulfide veins have been identified, 50 of them being economically significant. Most of these are referred to by numbers, e.g. ore vein 32 (Fig. 1), and a few by a place name, e.g. the Gaberovo vein system near the small village of Gaberovo (Fig. 1). The veins occur in a radial pattern possibly related to the existence of four fault sets (NW–SE, E–W, N–S and NE–SW; Atanasov 1959; Fig. 1). Veins trending NW–SW and E–W are the largest and most productive. Vein thickness varies considerably from half a meter to 30 m with 1 to 3 m being the average, whereas the strike length of the larger veins can be up to 4 km.

A general vertical zonation was established by Atanasov (1962) and Arnaudova et al. (1991), very similar to models of epithermal deposits, with base metals precipitating below precious metals (Buchanan 1981; Berger and Eimon 1983). The mineralised interval extends up to 1,500 m below the present land surface with the precious metal mineralization located in the uppermost 150–200 m. At the lowest levels, some veins pass into basement without observable change. Present-day vein outcrops were between 150 and 200 m below the palaeo-surface, which has been calculated by estimating the thickness of lava flows eroded from the central part of the volcano.

The predominant sulfides are pyrite, chalcopyrite, sphalerite and galena with minor Bi, Ag, Sb, As and Mo sulfides and native Au and Ag. Quartz is the dominant gangue mineral with lesser amounts of barite, chalcedony, jasper and calcite. The paragenesis is complex and six stages of mineralization have been identified by Breskovska and Tarkian (1993; Fig. 4). The third stage carries most of the galena and sphalerite, whereas most of the gold was deposited during the second and fourth stages. Gold occurs as small (1–100  $\mu\text{m}$ ) inclusions in quartz or in base metal

sulfides. Barite is found in stages three and four and calcite in stage six.

The mineralization and alteration fit neatly into the intermediate sulfidation category (Einaudi et al. 2003; Sillitoe and Hedenquist 2003) on the basis of tectonic setting, alteration and gangue minerals, key sulfides and metals, low Fe sphalerite (Breskovska and Tarkian 1993) and salinity of the ore fluids (see below), as proposed by Marchev et al. (2005).

#### Fluid inclusion micro-thermometry

**Materials and methods** Fluid inclusion data were obtained from surface and mine exposures of the main ore-bearing veins in the district. Altogether, 13 samples were selected for micro-thermometric studies and prepared as 100- to 200- $\mu\text{m}$ -thick doubly polished wafers. The measurements were carried out using a Linkham TH 600 heating–freezing stage calibrated with Analar grade chemicals.

**Petrography** The fluid inclusions studied occur in quartz and barite and are predominantly two-phase liquid vapour primary

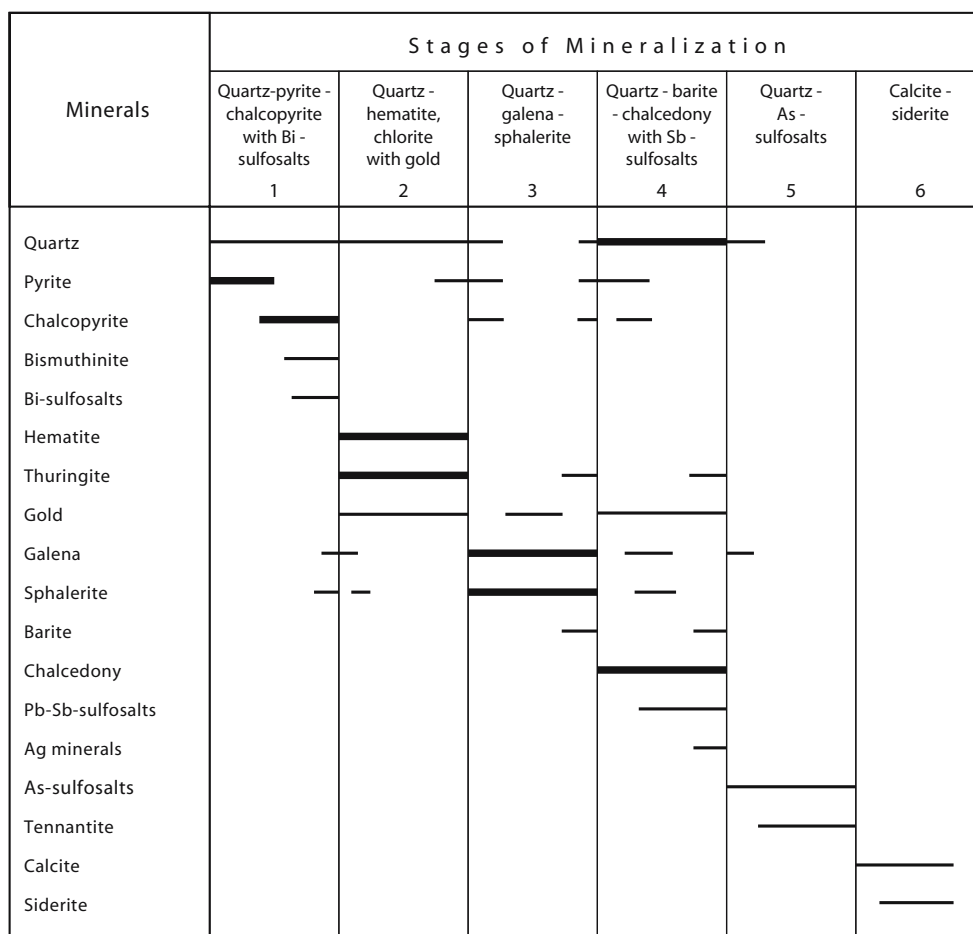


**Fig. 4** Paragenetic diagram illustrating stages of mineralization in the Madjarovo district. *Line width* indicates abundance. Simplified after Breskovska and Tarkian (1993)

inclusions. They are small, (<5–30 μm), and liquid-rich with the liquid content ranging from 85 to 45%. There is no evidence of necking. Based on Roedder’s (1984) criteria, all investigated fluid inclusions are identified as primary or pseudo-secondary. For some samples, especially quartz from the upper levels of the deposit, many inclusions are too small to measure (<5 μm), and so, the temperature of homogenisation (Th) and the temperature of final ice melting (Tm) measurements may have been derived from an unrepresentative population. Planes of secondary inclusions, mostly too small to measure, occur in some samples.

Typically, at depth, the quartz is associated with galena and sphalerite, whereas barite is the commonly associated mineral closer to the surface. Galena, sphalerite and barite are assigned to stages 3 and 4, respectively, in the paragenetic sequence described by Breskovska and Tarkian (1993; Fig. 4). Quartz samples from a barren quartz vein hosted by adularia–sericite alteration and two quartz–pyrite veins were also included in the study but the exact paragenetic positions of these are unknown.

**Homogenisation temperatures** Inclusions from quartz in veins containing galena and sphalerite (ore-stage quartz) homogenise at temperatures varying from about 160 to 320°C (Fig. 5; Table 1). The distribution of values is positively skewed. Fluid inclusions from co-existing quartz and barite homogenise over a similar range of temperatures to those in quartz co-existing with galena and sphalerite (160–320°C) but with a slightly lower mean (Fig. 5). However, the distribution in this case is normal. Inclusions in quartz from a barren vein (MJ 7/93) show similar values and a similar skewed distribution to those in ore-stage quartz. The skewed distributions might be artefacts due to the small number of samples and temperature variations in these complex epithermal systems. Fluid inclusions from a quartz–pyrite vein (OV2 4/92) show the widest temperature spread, from 157 to 356°C with a positively skewed distribution and a mean of 214°C. The highest homogenisation temperatures (~350°C) were recorded from quartz–pyrite veins from the upper part of ore vein 2. Temperatures of homogenisation

**Fig. 5** Histograms showing  
**a.** Homogenisation temperatures  
**(b).** Salinities. Data are sorted by vein type

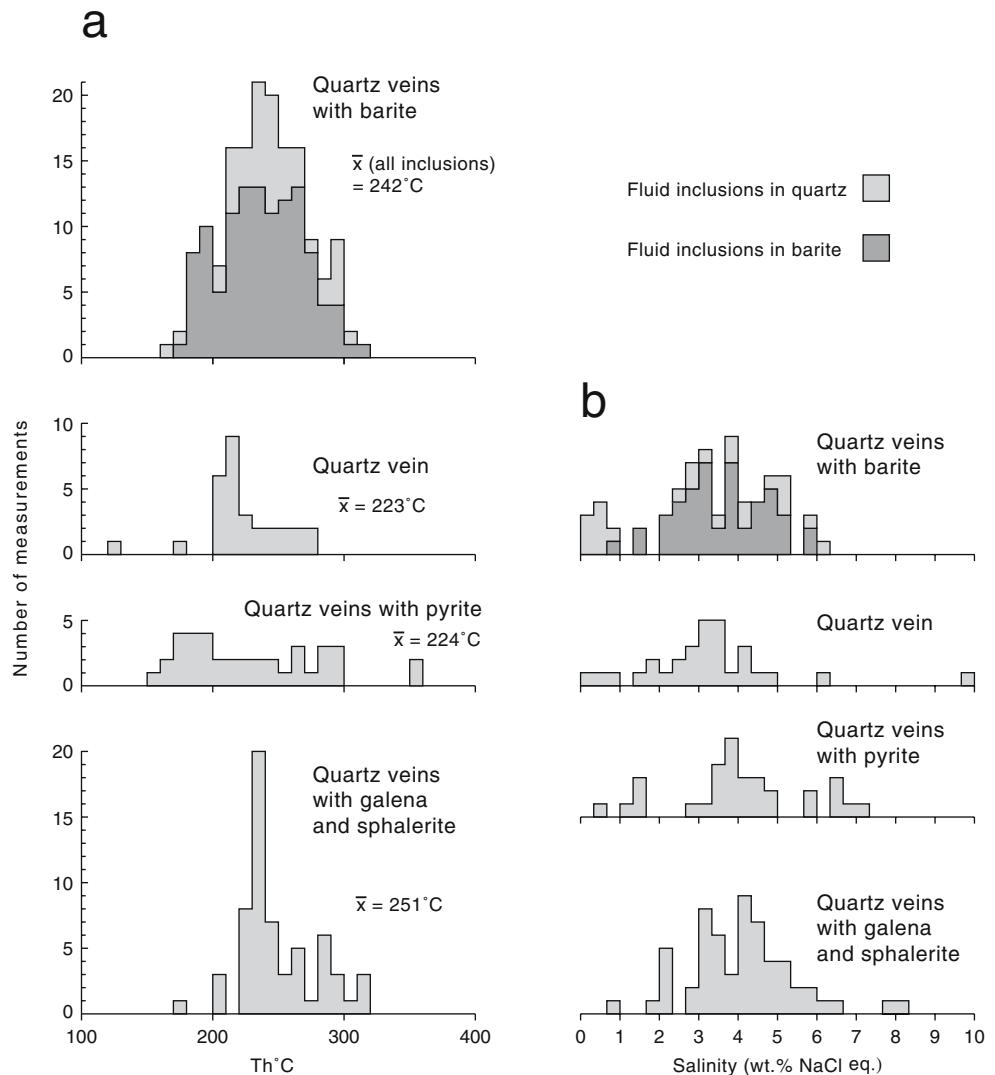


**Table 1** Summary of fluid inclusion data for main stage Pb–Zn mineralization and quartz-, barite- and pyrite-bearing veins

Sample	Elevation masl	Host mineral	Vein type (stage of mineralization, see Fig. 4)	Th°C			Tm°C		
				Mean (1 $\sigma$ )	Range	N	Mean	Range	N
MJ 7/93	640	Quartz	Quartz (?)	223(30)	128–279	30	–1.9	–0.1 to –5.9	30
OV32 1/93	531	Quartz	Quartz–barite (4)	226(31)	166–265	14	–0.9	0.0 to –2.9	14
OV32 1/93	531	Barite	Quartz–barite (4)	211(20)	172–252	11	–1.8	–1.2 to –2.7	11
GB 3/91	500	Barite	Quartz–barite–minor sulfides (4)	231(25)	185–266	14	–2.3	–1.4 to –3.1	4
GB 1/92	456	Quartz	Quartz–barite–galena–sphalerite (3/4)	278(26)	219–309	12	–2.7	–1.7 to –3.6	10
GB 1/92	456	Barite	Quartz–barite–galena–sphalerite (3/4)	233(20)	190–257	9	–2.7	–0.9 to –3.5	9
BR 3/92	400	Quartz	Quartz–galena–sphalerite (3)	255(34)	224–319	14	–1.9	–1.2 to –3.2	14
MJ 29/93	Approximately 400	Barite	Quartz–barite (4)	254(21)	212–299	27	–1.5	–1.8 to –3.0	3
MJ 33/93	Approximately 400	Barite	Quartz–barite(4)	233(29)	186–274	33	–2.2	–0.5 to –2.8	4
OV2 1/92	388	Quartz	Quartz–pyrite (?)	287(36)	240–350	5	–3.3	–2.8 to –3.8	2
OV2 4/92	375	Quartz	Quartz–pyrite (?)	214(45)	157–356	30	–2.3	–0.2 to –4.2	30
OV32 2/91	200	Quartz	Quartz–galena–sphalerite (3)	271(22)	221–297	8	–2.2	–1.1 to –3.4	5
OV15 2/93	165	Quartz	Chalcedony–barite (4)	238(11)	219–258	19	–2.9	–1.9 to –4.2	19
OV15 2/93	165	Barite	Chalcedony–barite (4)	259(36)	192–312	16	–2.1	–1.3 to –2.9	16
OV37 3/93	130	Quartz	Quartz–galena–sphalerite (3)	233(14)	202–281	27	–2.6	–1.3 to –4.9	27
OV2 5/92	105	Quartz	Quartz–galena–sphalerite (3)	260(34)	170–306	12	–2.1	–0.4 to –3.8	12

Sample locations given in Tables 2 and 6 except for OV32 2/91 ore vein 32, 200-m level, adit at GR 040122; BR 3/92 Brousevtsi mine, 400-m level, adit at GR 112050; GB 3/91 Gaberovo mine, 500-m level, adit at GR 098112. See Fig. 1 for grid references.

? Stage uncertain, masl meters above sea level, Th°C temperature of homogenisation, Tm°C temperature of final ice melting, N number of measurements

recorded by Breskovska and Tarkian (1993) for stages 3 and 4 compare well with data from this study but notably lack the high temperature tail (250–300°C) recorded here.

**Final melting temperatures** The final melting temperatures in ore-stage quartz range from –0.4 to –4.9°C (Table 1). These correspond to a low to intermediate salinity range of 1–8 wt% NaCl equivalent (Fig. 5). Inclusions in quartz–barite veins show a similar range of salinities but there is evidence for a separate population of very low salinity fluids (<1 wt%) in one sample (OV32 1/93). Inclusions in a quartz–pyrite vein (OV2 4/92) and a barren quartz vein (MJ 7/93) show similar salinity characteristics to those in ore-stage quartz. The highest salinity recorded at 10 wt% is from an inclusion in the barren quartz vein. Rare higher salinity inclusions (up to 18.4 wt% NaCl equivalents) were recorded from stages 4 and 5 by Breskovska and Tarkian (1993). Overall, there is little variation in fluid inclusion salinity between vein types. Values recorded by Breskovska and Tarkian (1993) are similar to the ones determined in the present study for stage 3 mineralization but rather lower for stage 4 (ca. 0–3 wt% NaCl equivalent).

**Evidence for boiling** The fluid inclusions from all samples studied in this research work show no evidence for boiling as defined by Bodnar et al. (1985). However, the inclusion populations lie close (over 80% of samples lie within the

mean and two standard deviations) to hydrostatic depth to boiling curves (Fig. 6). This is good evidence that most fluids boiled as is the presence of hydrothermal breccias and widespread adularia in the upper levels of the system. Boiling may also have occurred during the deposition of stage 2 mineralisation (Breskovska and Tarkian 1993). There is a suggestion that homogenization temperatures are varying more widely in the upper part of the deposit, from the palaeosurface to a depth of 500 m (Fig. 6). This has been observed in other epithermal deposits and attributed to homogenous and heterogenous trapping of a boiling fluid (Kiliyas et al. 2001; Scott and Watanabe 1998). We conclude from the foregoing that in this system the mean Th can be used as a measure of mineralizing temperatures, although this is not always the case (Naden et al. 2003; Bodnar et al. 1985).

Boiling may provide an alternative explanation for the high temperature tail seen in the inclusions from ore-stage quartz, barren quartz and quartz–pyrite veins. These may represent inclusions that have trapped a small and undetected amount of vapour (Kiliyas et al. 2001) as boiling commenced.

**Salinity versus temperature trends** Salinity versus temperature trends are presented for the different vein types (Fig. 7). The trends are similar for all vein types and show a linear, vertical, mostly continuous trend, indicating a

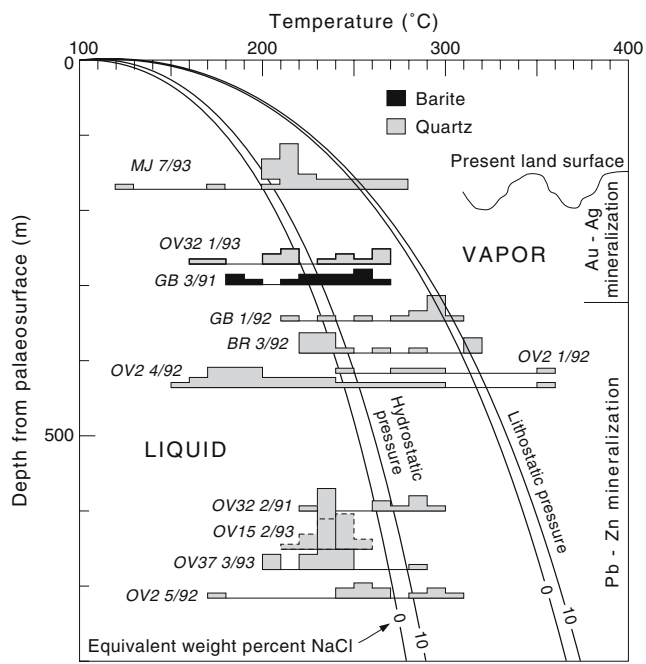


**Fig. 6** Depth below palaeosurface—Th plot for quartz and barite inclusion data from various vein types (Table 1). Palaeosurface estimated (see text) to be 150–200 m above the highest veins that are located at 660 m asl. Histograms are plotted with 10°C intervals. Superimposed on the diagram are hydrostatic and lithostatic depth to boiling curves for 0 and 10 wt% NaCl equivalent from Haas (1971). Co-existing barite and quartz show a similar distribution of Th values (Fig. 6a), and the former are not plotted for clarity. Depth intervals for precious and base metal mineralization are also shown

moderate change from low to intermediate salinity associated with small changes in temperature. These trends compare well with those recorded by Breskovska and Tarkian (1993) for stages 3 and 4. A similar trend was described from the Profitis Ilias gold deposit by Kiliyas et al. (2001) and explained in terms of mixing with an exotic brine (Simmons et al. 1988; Conrad et al. 1992) or extensive boiling and vaporisation of a low salinity fluid (e.g. Simmons and Browne 1997; Scott and Watanabe 1998). There is isotopic evidence for the presence of magmatic fluids in the system (see below) and also, as discussed above, evidence for boiling. We cannot distinguish between these two hypotheses, but there is no reason why both processes should not have operated. However, for boiling of a low salinity end member to cause the full range of salinities observed, open system boiling would be required, which is unusual in the upper parts of epithermal systems (Simmons and Browne 1997). Breskovska and Tarkian (1993) record a variety of salinity versus temperature trends for the other stages of mineralization, which indicate that adiabatic boiling and dilution of fluids occurred (Hedenquist and Henley 1985).

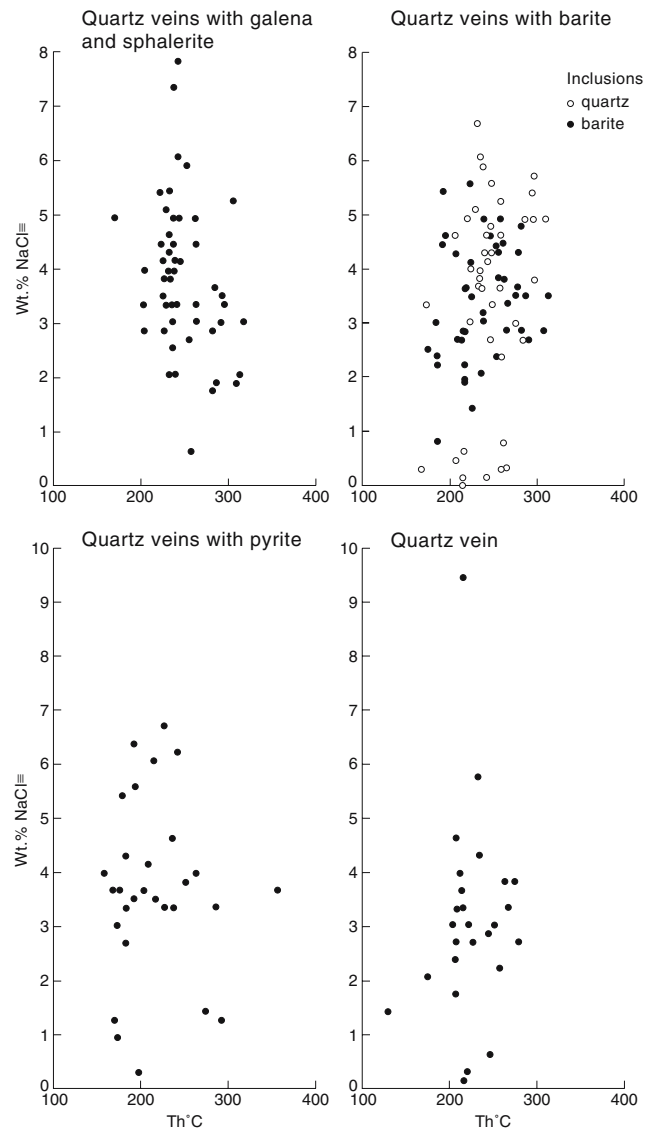


**Fig. 7** Homogenisation temperature versus salinity plots for various vein types

Age of mineralization and alteration

Radiometric ages on a variety of alteration minerals from Madjarovo in both high sulfidation and intermediate sulfidation assemblages fall into two groups of around 32 and 12 Ma (McCoyd, 1995, unpublished data; Marchev and Singer 2002). These data are taken to indicate by these authors that the mineralization and alteration occurred shortly after volcanism ceased and that there was a later regional hydrothermal event that partially reset the K–Ar systems in muscovite and alunite. Because of Ar loss by alunite, high sulfidation alteration has not been dated; however, cross-cutting relationships between vein mineralization and advanced argillic alteration in the central Harman Kaya monzonite intrusion suggest that vein

mineralization and intermediate sulfidation alteration post-date monzonite and lithocap formation. Adularia ( $^{40}\text{Ar}/^{39}\text{Ar}$ ) ages from vein mineralization ( $32.09 \pm 0.21$  Ma) are indistinguishable within experimental error from ( $^{40}\text{Ar}/^{39}\text{Ar}$ ) ages for the spatially associated monzonite stocks and quartz trachyte dykes ( $32.06 \pm 0.13$  Ma), indicating that the total duration of the late-stage magmatism and high and intermediate sulfidation systems was less than 310 ka (Marchev and Singer 2002).

## Methodology

**Silicate  $\delta^{18}\text{O}$ ,  $\delta D$**  To characterise the fluids responsible for the high and intermediate sulfidation alterations and the Pb–Zn mineralization, eight quartz and two sericite samples were collected from mainstage (stage 3) Pb–Zn veins and altered wallrocks, respectively, together with five samples of sericite and four of kaolinite from the main barren high sulfidation alteration. Quartz samples were separated by careful hand picking and were checked for purity by optical microscopy and X-ray diffraction (XRD). Kaolinite, sericite and pyrophyllite samples were separated and purified according to the method outlined by Hardy and Tucker (1988); all samples were checked for purity by XRD before analysis. Some sericite samples contained chlorite that was removed through warm 10% (v/v) HCl leaching. The samples were conventionally analysed for oxygen isotopic composition by a technique modified after that of Clayton and Mayeda (1963). Sample decomposition was carried out with bromine pentafluoride; the resultant oxygen reacted with graphite rods to produce carbon dioxide, the isotopic composition of which was determined using a VG SIRA 10 mass spectrometer. The accuracy of the technique was confirmed by the periodic analysis of the NBS-28 standard (African Glass Sand); the agreement with the accepted value of +9.6‰ was typically better than  $\pm 0.2\%$ .

Hydrogen isotope analyses were carried out on coarsely crushed samples of cleaned vein quartz. Splits of the samples (up to around 1 g) were washed in warm aqua regia and thoroughly rinsed in de-ionised water. The samples were then dried overnight under vacuum at 200°C before being run for  $\delta D$  following the technique of Fallick et al. (1987). For barite fluid inclusion analyses, the samples were purified using acid dissolution and heavy liquid separation. Splits of the samples (up to around 1 g) were then dried overnight at 120°C. Whereas quartz decrepitation temperatures in the quartz analyses exceeded 1100°C, barite decrepitation temperatures were kept below 450°C (to avoid sulphurisation of the evolved inclusion hydrogen). Quartz decrepitation was done in a degassed platinum crucible by induction heating, whereas barite was decrepitated in a step-heated furnace. Reproducibility of data by

this technique is considered to be no better than 5‰ based on our experience in the laboratory using natural samples. Silicate separates were analysed by a similar method, with reproducibility around  $\pm 3\%$  based on repeat analyses of the NBS-30 biotite standard (–65‰; Fallick et al. 1987).

**Sulfides** To characterise the sulphur isotope distribution in the deposits and to identify the most probable sulphur sources, a total of 27 sulfide analyses were carried out on vein samples and also on pyrite from altered vein wall-rocks. In addition, six whole rock samples from the central Rhodope basement were analysed. The vein and alteration pyrite were separated using a shaking table. The heavy mineral fraction so obtained was further enriched by handpicking before analysis. Whole rock sulphur was extracted according to the method of Canfield et al. (1986). Sulphur dioxide gas was extracted conventionally from all resulting sulfide separates following the method of Robinson and Kusakabe (1975). The gases were then run on a VG SIRA II mass spectrometer. Raw machine  $\delta^{66}\text{SO}_2$  data were converted to  $\delta^{34}\text{S}$  values by calibration with international standards NBS-123 (+17.1‰) and IAEA-S-3 (–31‰), as well as Scottish Universities Environmental Research Centre's (SUERC) internal lab standard CP-1 (–4.6‰). Reproducibility of the analytical results was checked through replicate measurements of these standards, resulting in a  $1\sigma$  reproducibility better than  $\pm 0.2\%$ . All sulphur isotope compositions were calculated relative to Canon Diablo Troilite (V-CDT) and are reported in standard notation.

**Sulfates** Four barite and two alunite samples were separated, respectively, from intermediate and high sulfidation veins by careful hand picking and were checked for purity by optical microscopy and XRD. Sulphur dioxide gas was extracted from the alunite (first converted to  $\text{BaSO}_4$  following the method of Wasserman et al. 1992) and barite following the method of Coleman and Moore (1978). The resultant gases were then processed in a similar way to that used for sulfides (see above).

Oxygen isotope analyses were carried out on barite and converted alunite samples following the method described by Hall et al. (1991). Carbon dioxide released by this method was analysed on a VG SIRA 10 mass spectrometer. Three repeat analyses of the NBS 127 standard ran during the analytical phase gave results of +9.4, +9.5 and +9.6‰ versus an estimated accepted value of +9.3‰; thus, whilst precision is excellent for this technique, the data appear to be slightly higher than the average inter-laboratory mean. However, the  $2\sigma$  value for the standard used in inter-laboratory comparison is  $\pm 0.4\%$  (variation in mean of means from contributing labs), and so the data are presented as measured.

**Table 2** Results of the  $\delta^{18}\text{O}$ – $\delta D$  study for silicate samples from Madjarovo (data are relative to V–SMOW)

Sample	Mineral	$\delta^{18}\text{O}\%$	$\delta D\%$	Rock type	Location
OV2 1/92	Qtz	13.5	–43.6	Banded qtz–minor pyrite vein	Ore vein 2–388 m level (GR 042 138)
OV2 4/92	Qtz	10.9	–60.5	Quartz–minor pyrite vein	Ore vein 2–375 m level (adit at GR 042 138)
OV2 5/92	Qtz	8.5	–67.7	Quartz–galena–sphalerite vein	Ore vein 2–150 m level (adit at GR 042 138)
OV15 2/93	Qtz	9.5	–60.1	Chalcedony–barite vein	Ore vein 15 (Drill core from approximately GR 092 1)
OV32 1/93	Qtz	11.9	–72.1	Quartz–barite vein	Ore vein 32 (approximately GR 040 100)
OV37 3/93	Qtz	9.9	–78.6	Quartz–galena–sphalerite vein	Ore vein 37 (adit at GR 023 113)
GB 1/92	Qtz	10.7	–62.8	Qtz–galena–sphalerite–barite vein	Gaberovo vein system–456 m level (adit at GR 098 112)
MJ 7/93	Qtz	10.4	–71.0	Quartz vein	GR 030 116
MJ 7a/93	Ms	10.1	–77.0	Sericite alteration to qtz vein MJ 7/93	GR 030 116
RG 11/91	Ms	8.5	–63.6	Quartz–sericite alteration	GR 039 125
RG 14/91	Ms	8.0	–54.3	Sericitic alteration	GR 056 093
MJ 1/93	Ms	7.9	–72.5	Sericitic alteration	GR 059 099
MJ 12/93	Ms	7.5	–59.6	Argillic alteration, some sericite	GR 042 104
MJ 14b/93	Ms	7.1	–62.7	Sericitic alteration	GR 042 104
MJ 26/93	Ms	7.6	–65.6	Sericitic alteration	GR 049 102
MJ 28a/93	Kln	11.9	–76.2	Kaolinite veinlets	GR 053 104
MJ 28b/93	Kln	9.4	–74.9	Kaolinite veinlets	GR 053 104
ST 3/93	Kln	6.9	–67.6	Advanced argillic alteration	GR 060 095
ST 4/93	Kln	8.9	–69.7	Advanced argillic alteration	GR 060 095

The first ten samples are from veins and alteration related to intermediate sulfidation Pb–Zn mineralization; the remainders are from high sulfidation alteration. The grid references for locations are in Fig. 1.  $\delta D$  for quartz are measured FI values.  $\delta D$  for other silicates are calculated mineral values. Sheppard and Gilg (1996) provide an isotopic equilibrium fractionation between the sericite/muscovite of –25‰ across the range of temperatures under consideration. The fractionation of hydrogen isotopes between kaolinite and water is from Gilg and Sheppard (1996). *Qtz* quartz, *Ms* muscovite, *Prl* pyrophyllite, *Kln* kaolinite

Alunite hydrogen isotope composition was determined by a modified procedure after Godfrey (1962). Thermal decomposition temperature was controlled by step heating (max=550°C) to minimise the potential of  $\text{SO}_2$  and  $\text{H}_2\text{SO}_4$  release (Wasserman et al. 1992). The laboratory light standard (a bulk local winter meteoric water) was used to calibrate these data, with an accepted value of –94‰ versus Vienna Standard Mean Ocean Water (V–SMOW), and an error of reproducibility around  $\pm 2\%$ .

## Results

**Silicates** Quartz from the Pb–Zn veins yields  $\delta^{18}\text{O}$  values of +8.5 to +13.5‰ and  $\delta D$  values of –43.6 to –78.6‰. Intermediate sulfidation and high sulfidation alteration

sericite is characterised by similar  $\delta^{18}\text{O}\%$  (+5.2 to +10.1 and +7.1 to +8.0‰) and  $\delta D\%$  (–36.3 to –77.0 and –36.3 to –72.5‰) values. Kaolinite yields  $\delta^{18}\text{O}$  values of +6.9 to +11.9‰ and  $\delta D$  values of –67.6 to –76.2‰ (Table 2).

**Sulfides**  $\delta^{34}\text{S}$  values of whole rock, alteration pyrite and vein sulfide samples are –6.8 to +4.8‰ (mean=0.2 $\pm$ 4.2‰,  $1\sigma$ ,  $n=6$ ), +1.1 to +6.8‰ (mean=+4.3 $\pm$ 1.8‰,  $1\sigma$ ,  $n=7$ ) and –1.2 to +6.8‰, respectively (Tables 3, 4, and 5; Fig. 8). All five producing vein systems were investigated, and whereas the mean of all  $\delta^{34}\text{S}$  vein sulfide values is +2.8 $\pm$ 2.5‰ ( $1\sigma$ ,  $n=20$ ; range, –1.2 to +6.8‰), there is a clear sulphur isotopic distinction between the main veins hosted by the volcanic sequence and the Brusevtsi vein system located 6 km southwest of the main occurrences and hosted by the metamorphic sequence (Figs. 1 and 8). The latter has a mean  $\delta^{34}\text{S}$  value of +5.2 $\pm$ 1.3‰. ( $1\sigma$ ,  $n=8$ ) versus the

**Table 3** Sulfur isotope data for whole rock samples from the Central Rhodopes

Sample	$\delta^{34}\text{S}_{\text{V-CDT}}\%$	Location	Rock type
MD 4/92	–1.64	Ca. 1.5 km north of Madan. Roadside exposure	Gneiss
MD 6/92	3.56	Ca. 3.0 km north of Madan. Roadside exposure	Schist
MD 7/92	4.78	Ca. 3.0 km north of Madan. Exposure approximately 500 m from road.	Amphibolite
SU 1/92	–6.77	Ca. 45 km south west of Madjarovo	Pyroxene gneiss
LK 2/92	1.56	Ca. 2 km north of Djurkovo village <sup>a</sup>	Gneiss
LK 3/92	–0.03	Ca. 2 km north of Djurkovo village <sup>a</sup>	Gneiss

<sup>a</sup> Djurkovo village is in the Luky ore field 90 km NW of Madjarovo.

**Table 4** Sulfur isotope data for alteration pyrite from Madjarovo

Sample	$\delta^{34}\text{S}_{\text{V-CDT}}\text{‰}$	Alteration	Location
RG 14/91	4.89	Sericite (HS)	GR 056 093
RG 11/91	2.83	Qtz-sericite (IS)	GR 039 125
RG 12B/91	1.08	Propylitic (IS)	GR 063 133
RG 20/91	6.80	Siliceous (IS)	GR 081 136
MJ 1/92	5.03	Sericite (HS)	GR 059 099
MJ 2/92	4.89	Siliceous (IS)	GR 069 128
RG 19/91	4.27	Siliceous (IS)	GR 075 129

Grid references for locations in Fig. 1.

HS High sulfidation, IS intermediate sulfidation

overall volcanic-hosted vein  $\delta^{34}\text{S}$  mean value of  $+1.2 \pm 1.7\text{‰}$  ( $1\sigma$ ,  $n=12$ ).

**Sulfates** Barite  $\delta^{34}\text{S}$  values show restricted variation in the  $+21.4$  to  $+23.1\text{‰}$  range, with a mean value of  $+22.5 \pm 0.7\text{‰}$  ( $1\sigma$ ,  $n=9$ ), whereas barite  $\delta^{18}\text{O}$  values range from  $+5.8$  to  $+8.1\text{‰}$ . Alunite has similar  $\delta^{34}\text{S}$  values ( $+22.2$  and  $+24.9\text{‰}$ ,  $n=2$ ), with  $\delta^{18}\text{O}$  values more elevated than for barite ( $+10.1$  and  $+11.6\text{‰}$ ,  $n=2$ ). Barite fluid inclusion  $\delta D$  values

range from  $-58.4$  to  $-67.1\text{‰}$  ( $n=6$ ), whereas the two alunite samples have distinctly different  $\delta D$  values close to  $-36\text{‰}$  (Table 6).

## Discussion

**Source of sulfide sulphur** Sulfide in the vein and alteration systems at Madjarovo ranges in  $\delta^{34}\text{S}$  values from around  $-1$  to  $+7\text{‰}$  (Fig. 8). The geological setting allows for three possible sulphur sources at Madjarovo: igneous sulphur, remobilised igneous sulphur from the volcanic rocks (essentially indistinguishable from igneous sulphur) and remobilised crustal sulphur.

Sulphur isotope data for Madjarovo volcanic and intrusive rocks are not available. However, compositionally similar rocks from the nearby Borovitsa shoshonitic volcanic rocks, 30 km west of Madjarovo, show values varying between  $-9.9$  and  $+8.2\text{‰}$  with most samples, except rhyolites, having positive values (Marchev and Popov, 1990, unpublished data). Madjarovo metamorphic

**Table 5** Sulfur isotope data for vein sulfides from Madjarovo and calculated  $\text{H}_2\text{S}$  data in equilibrium with measured sulphide mineral data, using the temperatures derived from associated quartz fluid

Sample	Mineral	$\delta^{34}\text{S}_{\text{CDT}}\text{‰}$	Temperature ( $^{\circ}\text{C}$ )	Calculated $\delta^{34}\text{S}_{\text{H}_2\text{S}}$	Location
OV2 3/92	Galena	0.1	244 <sup>a</sup>	2.5	Ore vein 2–420 m level (adit at GR 042 138)
OV2 4/92	Pyrite	5.5	214 <sup>b</sup>	3.8	Ore vein 2–375 m level (adit at GR 042 138)
OV2 5/92	Galena	0.3	260 <sup>b</sup>	2.5	Ore vein 2–150 m level (adit at GR 042 138)
OV2 5/92	Pyrite	1.1	260 <sup>b</sup>	-0.3	
OV2 5/92	Sphalerite	0.8	260 <sup>b</sup>	0.5	
OV3 1/92	Chalcopyrite	1.1	244 <sup>a</sup>	1.1	Ore vein 3–35 m level (shaft at approximately GR 058 122)
OV3 1/92	Galena	-1.2	244 <sup>a</sup>	1.2	
OV3 1/92	Sphalerite	1.1	244 <sup>a</sup>	0.7	
OV3 1/92	Chalcopyrite	1.0	244 <sup>a</sup>	1.0	
OV58 1/92	Galena	1.5	244 <sup>a</sup>	3.9	Ore vein 58–495 m level (adit at GR 031 110)
BR 1/91	Galena	3.1	255 <sup>c</sup>	5.4	Brusevtsi vein system–350 m level (adit at GR 112 050)
BR 1/91	Pyrite	6.2	255 <sup>c</sup>	4.8	
BR 1/91	Sphalerite	5.1	255 <sup>c</sup>	4.7	
BR 1/91	Chalcopyrite	5.1	255 <sup>c</sup>	5.1	
BR 3/91	Galena	3.6	255 <sup>c</sup>	5.9	Brusevtsi vein system–350 m level (adit at GR 112 050)
BR 3/91	Sphalerite	5.5	255 <sup>c</sup>	5.1	
BR 3/91	Phyrite	6.5	255 <sup>c</sup>	5.1	
BR 3/91	Phyrite	6.8	255 <sup>c</sup>	5.4	
GB 1/92	Sphalerite	2.8	260 <sup>d</sup>	2.5	Gaberovo vein system–456 m level (adit at GR 098 112)
GB 1/92	Galena	0.3	260 <sup>d</sup>	2.4	

The mineral– $\text{H}_2\text{S}$  fractionations were calculated using the equations in Ohmoto and Rye (1979). Grid references for locations are in Fig. 1.

<sup>a</sup> Average of all mean FI temperatures

<sup>b</sup> Average FI temperature

<sup>c</sup> Average FI temperature of single sample from the Brusevtsi vein

<sup>d</sup> Calculated sphalerite–galena equilibrium temperature

### Histograms of all sulfide S isotope data, Madjarovo area

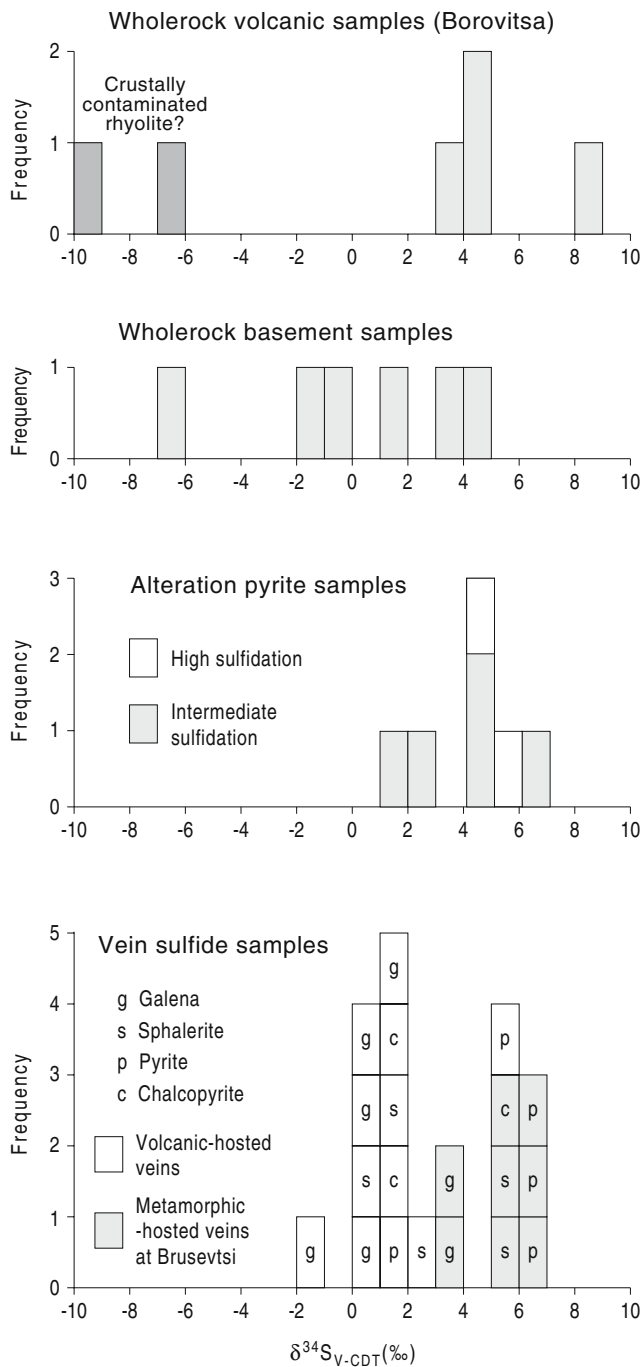


**Fig. 8** Histograms of sulfide S isotope data from all investigated wholerocks, alteration pyrite and vein sulphide samples, Madjarovo district

basement rocks have a  $\delta^{34}\text{S}$  range of  $-6.8$  to  $+4.8\text{‰}$ . A simple comparison between the three sets of values shows a large degree of overlap (Fig. 8).

In each vein system, the paragenesis is dominated by sulfides with no sulfate present in the quartz–sulfide veins.

Under the physical and chemical conditions ( $T < 300^\circ\text{C}$ , low pH and Eh) envisaged for the main stage fluids the major sulphur species would be  $\text{H}_2\text{S}$  (Ohmoto and Rye 1979). At these temperatures, sulfide dominance results in sulfide mineral  $\delta^{34}\text{S}$  values being close to the original fluid  $\delta^{34}\text{S}_{\text{H}_2\text{S}}$  (Ohmoto and Rye 1979). We have calculated the  $\delta^{34}\text{S}_{\text{H}_2\text{S}}$  in equilibrium with each mineral for appropriate temperatures (Table 5) and plotted these values from the main vein systems in Fig. 9. As with sulfide mineral  $\delta^{34}\text{S}$ , there is a clear S isotopic distinction between the volcanic- and basement-hosted veins. Whilst our basement  $\delta^{34}\text{S}$  data (see above) essentially overlap the range of the vein data, the significant distinction between the volcanic-hosted veins ( $\sim +1\text{‰}$ ) and the heavier ( $\sim +5\text{‰}$ )  $\delta^{34}\text{S}$  values of the basement-hosted Brusevtsi vein system points to a possible variation in the source or chemistry at the time of deposition. A more primitive value, i.e. nearer  $0 \pm 4\text{‰}$ , is anticipated for primary magmatic sulfide (Ohmoto and Rye 1979), and this is consistent with volcanic-hosted vein data. On the basis of these data alone, however, it is not possible to determine if this sulphur is magmatically derived, or remobilised from the volcanic host rocks: Data are consistent with either source. By contrast, the suggestion is made that the basement-hosted veins may have incorporated remobilised sulfide from basement rocks. It is noteworthy to mention that the  $\delta^{34}\text{S}$  values of the vein and replacement deposits hosted by the basement west of Madjarovo at Madan (mean  $\delta^{34}\text{S}$  value of  $4.4\text{‰}$ ) and Laki (mean  $\delta^{34}\text{S}$  value of  $5.4\text{‰}$ ) also show relatively high  $\delta^{34}\text{S}$ , comparable with that at Brusevtsi (McCoyd, 1995, unpublished data).

**Source of sulfate sulphur** The  $\delta^{34}\text{S}$  values for barite and alunite are closely grouped and lie between  $+20$  and  $+25\text{‰}$ . Although the estimated value for Miocene seawater sulfate (Claypool et al. 1980,  $\delta^{34}\text{S} \approx 20\text{‰}$ ) lies close to that observed in the barite and alunite samples and the paleogeography permits a marine influence (see above), we do not believe that these data reflect a sea water sulfate contribution. This conclusion is based on the  $\delta^{18}\text{O}$  and  $\delta D$  values of barite and alunite that show no evidence of a seawater contribution to the system (see fluid section below). Any significant contribution of seawater should be reflected also in the other isotope systems (e.g. Pflumio et al. 1991).

Instead, we believe that the sulfate sulphur was derived from the disproportionation of  $\text{SO}_2$  in the volcanic system at high  $\text{H}_2\text{S}/\text{SO}_4$  ratios (Rye et al. 1992; Rye 1993). Wholesale oxidation of sulfide to sulfate results in no fractionation effect with the resultant sulfate inheriting the value of the  $\delta^{34}\text{S}_{\text{H}_2\text{S}}$  of the hydrothermal fluid. Such a process cannot explain the observed  $\delta^{34}\text{S}$  values for barite and alunite. However, if equilibrium is established between sulfide and sulfate, then fractionation will occur. The

**Table 6** Stable isotope characteristics of vein barite and alunite (prefix AL) from Madjarovo

Sample	$\delta^{34}\text{S}_{\text{V-CDT}}\text{‰}$	$\delta^{18}\text{O}_{\text{V-SMOW}}\text{‰}$	$\delta D\text{‰}$	Location
MJ 29/93	22.6	5.8	-63.7	Ore vein 2 (approximately GR 043 138)
MJ 33/93	22.7	6.3	-67.1	Ore vein 2 (approximately GR 043 138)
GB 1/92	23.1	8.0	-65.2	Gaberovo vein system, 456-m level (adit at GR 098 112)
OV32 1/93	21.4	8.1	-58.4	Ore vein 32 (approximately GR 040 100)
AL 1/91	24.9	11.6	-35.1	GR 062 101
AL 1/92	22.2	10.1	-36.0	GR 063 102

$\delta D$  for barite and alunite are measured FI and mineral values, respectively. The grid references for locations are in Fig. 1.

average  $\delta^{34}\text{S}$  value of vein-hosted sulfide is +1‰, whereas the average sulfate  $\delta^{34}\text{S}$  value is +22.5‰. Using the equation of Ohmoto and Rye (1979), this gives a formation temperature of around 280°C, which is consistent with other estimates for depositional temperature of base-metal veins and high sulfidation alteration and strongly suggests that equilibrium was established. Disproportionation of  $\text{SO}_2$  below about 400°C in magmatic hydrothermal systems produces  $\text{H}_2\text{SO}_4$  and  $\text{H}_2\text{S}$ , and equilibrium sulphur isotope fractionation can lead to the values observed in Madjarovo barite and alunite (Rye et al. 1992). The  $\text{H}_2\text{S}/\text{SO}_4$  ratio is critical in determining the absolute  $\delta^{34}\text{S}$  of each species: The higher the ratio, the closer the sulfide value to the overall isotopic composition of the hydrothermal system

and vice versa. We, therefore, suggest that, in the deeper parts of the mineralizing system at Madjarovo, the ratio of  $\text{H}_2\text{S}/\text{SO}_4$  was high, dominated by sulfide. This would produce sulfate with high  $\delta^{34}\text{S}$ . A proportion of this component survived the deposition of sulfide in the deep vein system to continue depositing barite at higher levels.

Furthermore, combining the  $\delta^{34}\text{S}$ ,  $\delta^{18}\text{O}_{\text{SO}_4}$  and  $\delta D$  values of investigated alunite (Fig. 10d) and by comparing them with Rye et al.'s (1992) data indicates a magmatic hydrothermal origin for this species. A meteoric water component may have influenced the deposition, but based on two points only, this conclusion cannot be definitive. Undoubtedly, there was a significant meteoric influence in the fluids depositing the barite, given the similarity between the barite isotopic data and that for the quartz from the Pb–Zn veins as discussed below (Fig. 10d).

Further evidence that supports a magmatic origin for the high sulfidation alteration at Madjarovo includes the presence of zunnyite and high  $\text{PO}_4$  levels in alunite (Velinov and Nokov 1991). Other diagnostic features include the presence of vuggy silica and the near vertical, pod-like nature of the alteration zones (Hedenquist et al. 1996). The acid-sulfate alteration at Madjarovo is not typical in this respect, as vuggy silica is poorly developed. However, in its overall morphology, the alteration does tend towards being near vertical and pod-like. A large difference in the observed values for the pyrite and alunite sulphur isotopes as seen at Madjarovo (below) is also thought to be diagnostic of a magmatic hydrothermal environment (Rye et al. 1992). On the other hand, coarsely crystalline alunite that is typical of a magmatic steam origin has not been seen. In fact, achieving a uniquely magmatic isotope

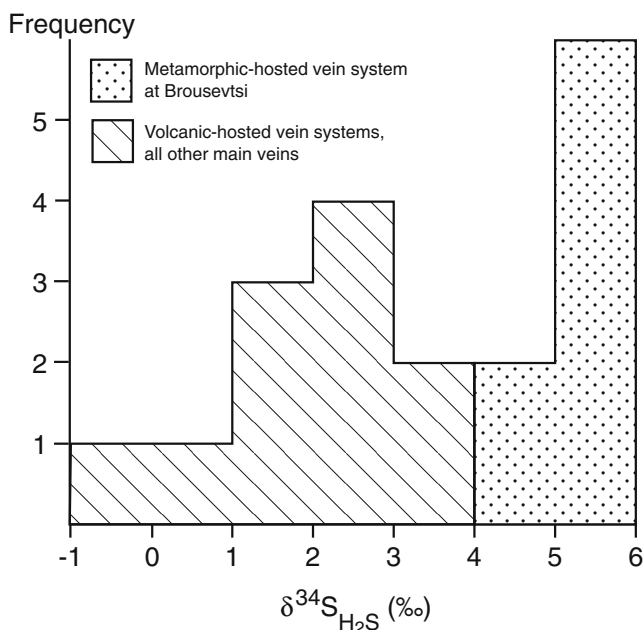
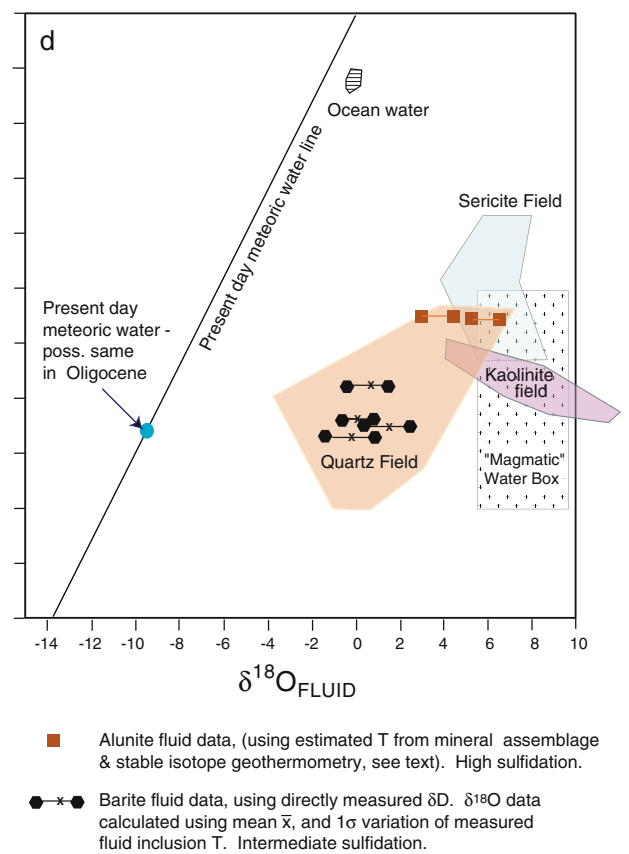
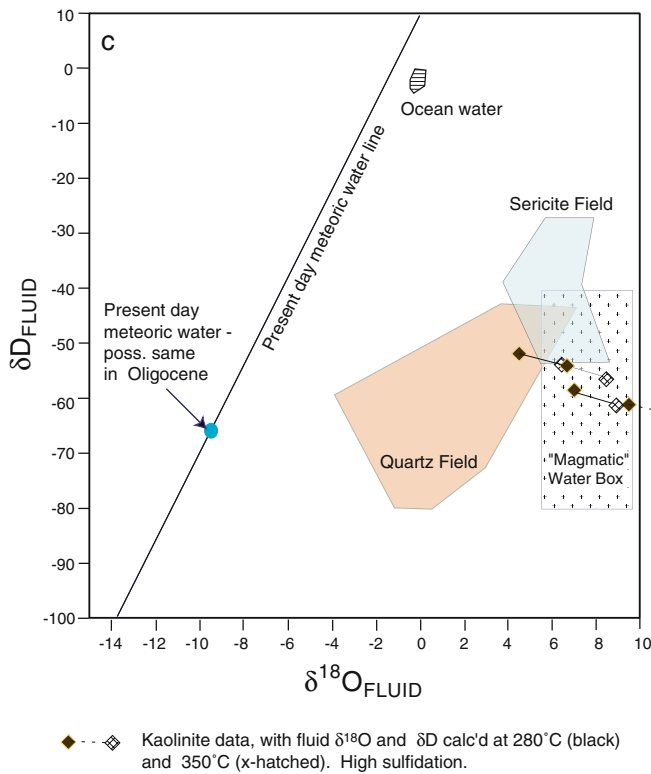
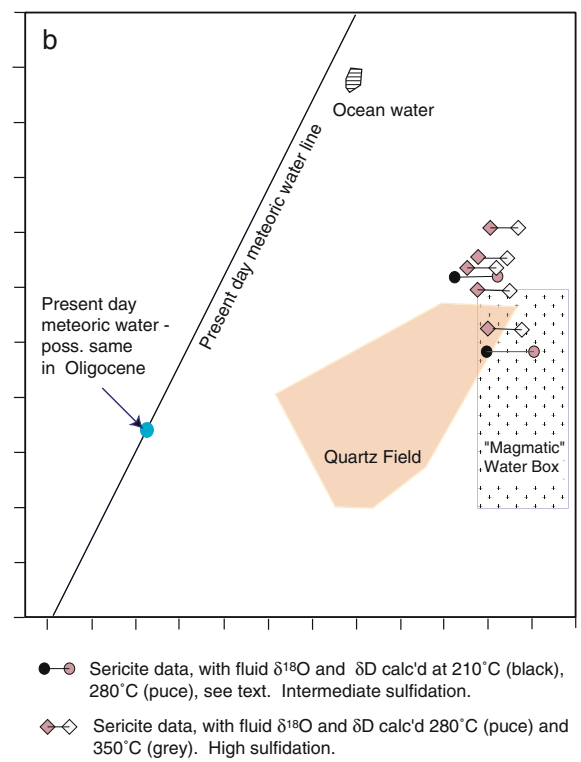
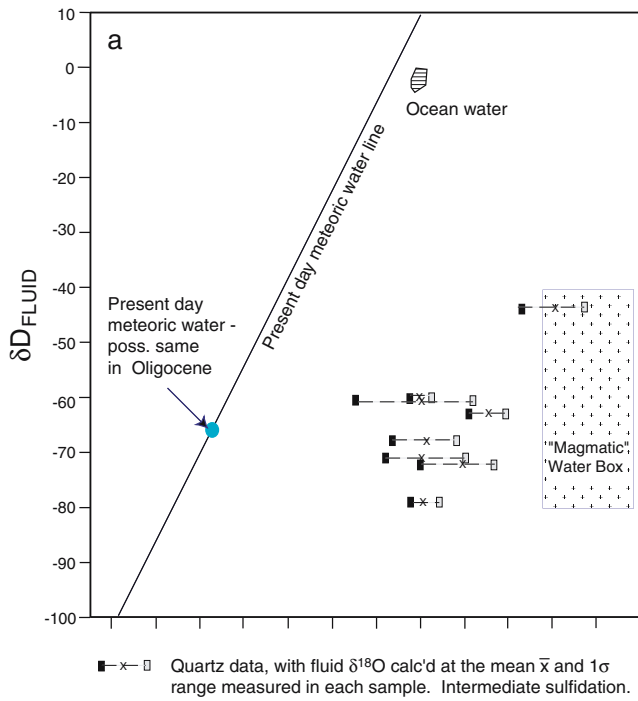


**Fig. 9** Histogram of  $\text{H}_2\text{S}$   $\delta^{34}\text{S}$  in equilibrium with each sulfide at a given temperature (using either the average temperature of associated quartz fluid inclusions, or the equilibrium temperature of sphalerite and galena in same hand specimen, using the Rye 1974 equation). The mineral– $\text{H}_2\text{S}$  fractionations were calculated using the equations in Ohmoto and Rye (1979). The difference in the measured values between the centrally placed vein systems and the outlying Brousevti vein system is reflected by this plot

**Fig. 10** Plots of various Madjarovo hydrothermal systems in  $\delta D$ – $\delta^{18}\text{O}$  space. **a** Calculated fluid in equilibrium with measured  $\delta^{18}\text{O}_{\text{Qtz}}$  versus directly measured fluid inclusion  $\delta D$  for intermediate sulfidation Pb–Zn veins. **b** Calculated fluid in equilibrium with measured  $\delta^{18}\text{O}$  versus calculated  $\delta D$  for sericites from intermediate sulfidation Pb–Zn veins and high sulfidation alteration. **c** Calculated fluid in equilibrium with measured  $\delta^{18}\text{O}$  versus calculated  $\delta D$  for kaolinite from high sulfidation alteration. **d** Calculated fluid in equilibrium with measured  $\delta^{18}\text{O}$  and  $\delta D$  in alunite and with measured  $\delta^{18}\text{O}$  versus directly measured fluid inclusion  $\delta D$  for barite



signature would require an unreasonably high temperature in excess of 350°C, which is not supported by the mineral assemblages. The obvious source for the volatiles would be the monzonite intrusions found in close proximity to the acid-sulfate alteration.

**Source of fluids** This section discusses the fluids involved in the genesis of main stage Pb–Zn mineralization and associated wallrock alteration, and the high level and central high sulfidation alteration. The temperature range used in the calculations for high sulfidation alteration (280–350°) is discussed above. The temperature ranges for intermediate sulfidation quartz are based on the mean $\pm 1\sigma$  for each sample (Table 1), and the range for intermediate sulfidation sericite is mean $\pm 1\sigma$  for quartz veins with galena and sphalerite (210–280°).

**Quartz associated with Pb–Zn veins:** This quartz has an intimate association with the economic minerals and so bears directly on their origin. Fluids in equilibrium with measured quartz  $\delta^{18}\text{O}$  values and directly measured fluid inclusion  $\delta D$  are plotted in Fig. 10a. The data lie in a cluster to the left of the commonly accepted magmatic water box

(Sheppard 1986) and adjacent to the estimated value for local Oligocene meteoric water. A fundamental question to ask of these systems is to what extent is this distribution the result of boiling, cooling, mixing or water–rock interaction of a meteoric fluid (e.g. Cooke and McPhail 2001).

#### Boiling, cooling or mixing?

To constrain the nature of the process/es involved in this deposition, we have quantitatively modelled the isotopic effects of cooling, boiling and mixing (Fig. 11) using the quartz  $\delta^{18}\text{O}$  data after the method of Wagner et al. (2005). For the calculated mixing lines, we have used reasonable end-member  $\delta^{18}\text{O}$  values of +7.5‰ for fluids in equilibrium with the magmatic epithermal end member and –9.5‰ for estimated local Oligocene meteoric waters. The temperature of the meteoric end member is varied between 50 and 200°C to mirror natural systems and take account of typical measured fluid inclusion temperatures of this system. The mixing lines, boiling and cooling curves plot the values of the measured  $\delta^{18}\text{O}$  of quartz precipitating

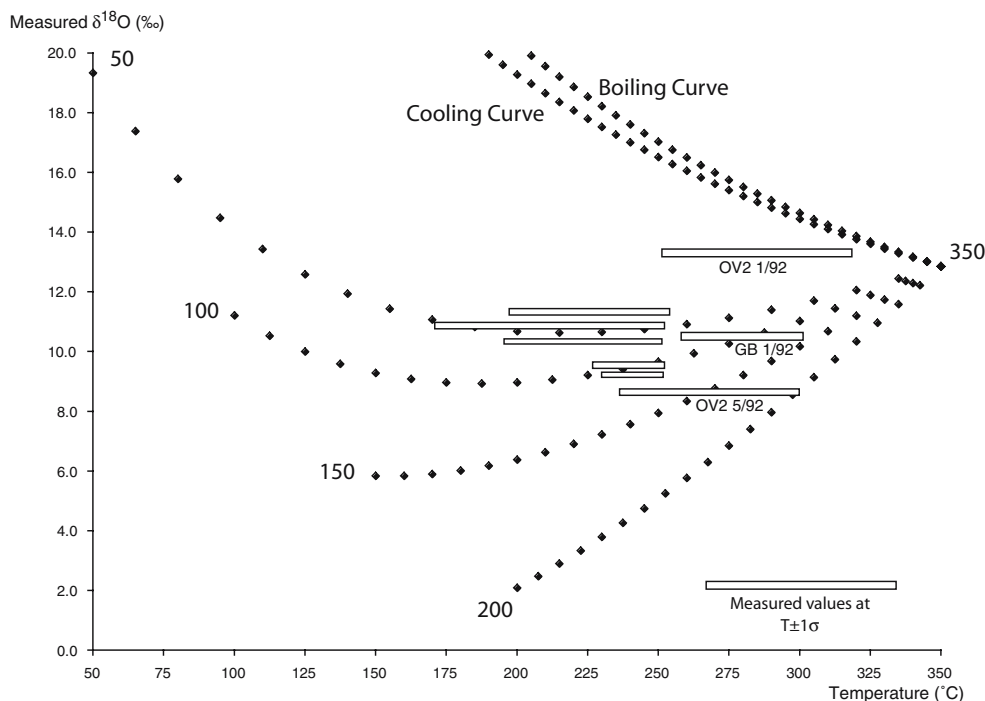


**Fig. 11** Plot of calculated mixing lines between magmatic end member (with fluid  $\delta^{18}\text{O}=+7.5\text{‰}$ ) at 350°C and meteoric water (fluid  $\delta^{18}\text{O}=-9.5\text{‰}$ ), cooling and boiling curves (using magmatic fluid  $\delta^{18}\text{O}$  end member of +7.5‰). The temperature of the meteoric end member is varied between 50 and 200°C to mirror natural systems and account for typical measured fluid inclusion temperatures of this system. The mixing, boiling and cooling curves plot the values of measured  $\delta^{18}\text{O}$  of quartz precipitating from each process. Boxes represent the actual measured values of quartz in the system, plotted against the mean values ( $\pm 1\sigma$ ) of the fluid inclusion temperatures from each sample.

Measured data do not fit the cooling or boiling curves. Most of the data fall on mixing trends with about 50:50 magmatic to meteoric input; another two, GB 1/92 and OV2 5/92, show greater input of magmatic water. One sample sticks out—OV2 1/92. We consider this sample to be the closest end member to the magmatic fluid. Changing the parameters of the modelling to higher fluid  $\delta^{18}\text{O}$  or lower meteoric  $\delta^{18}\text{O}$  (neither of which is unreasonable in a natural system of the time scale of this system), the samples would plot closer to the mixing lines—in all cases near the magmatic end member. Modelling based on Wagner et al. (2005)

from each process, super-imposed upon which are the actual measured values. The measured data do not fit the cooling or boiling curves. Instead, most of the data fit on mixing trends, with about 50:50 magmatic to meteoric input; another two show greater input of magmatic water. One sample sticks out on Figs. 11 and 10a–OV2 1/92. We consider this sample to be the closest end member to the magmatic fluid. Changing the parameters of the modelling to higher fluid  $\delta^{18}\text{O}$  or lower meteoric  $\delta^{18}\text{O}$  (neither of which is unreasonable in a natural system on the time scale of this system), the sample would plot closer to the mixing lines—in all cases near the magmatic end member. This sample is from a quartz–pyrite vein in the upper part of the ore vein 2 system, which contains some of the highest temperature fluid inclusions (Table 1); otherwise, the sample is not geologically or mineralogically distinctive.

Water rock reactions

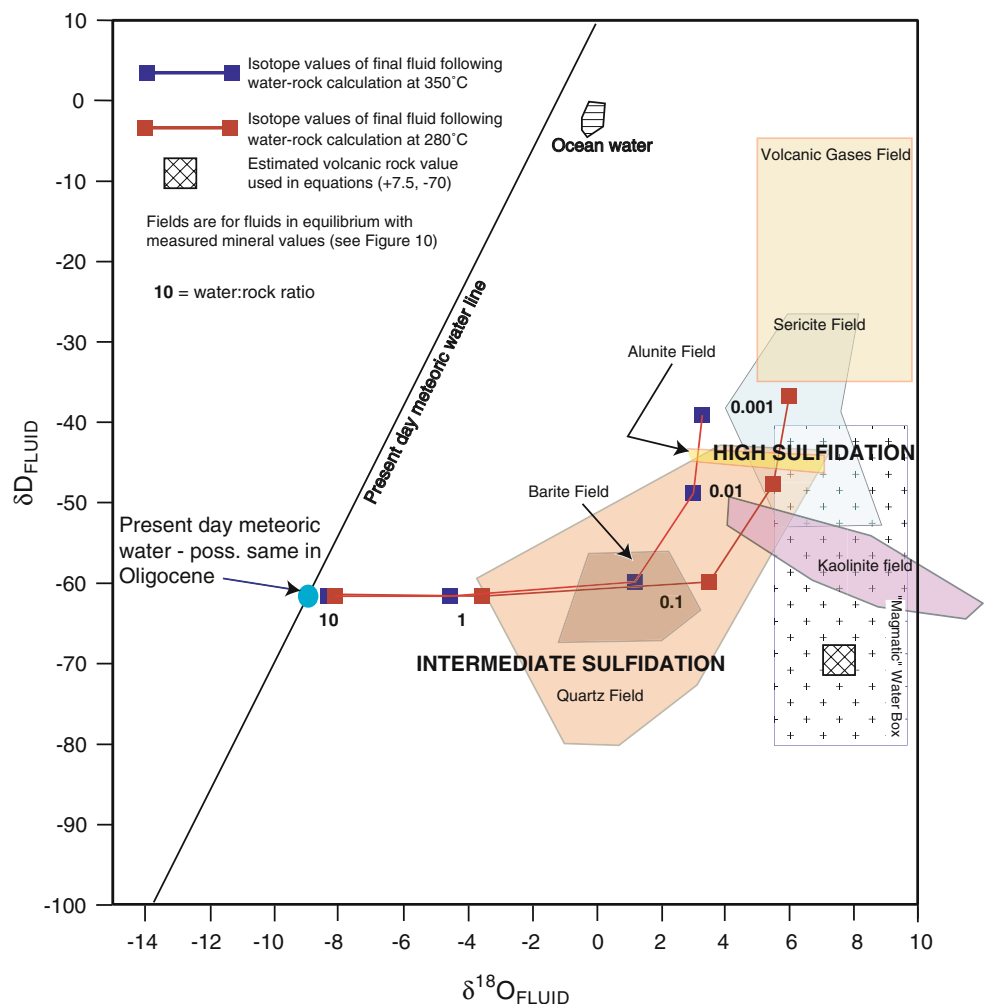
It is reasonable to ask if the trajectory of the quartz fluid data is the result of local meteoric water interacting with the host

rocks at varying water–rock ratios and temperature. Following the classic method of Field and Fifiarek (1985), we have plotted likely trajectories for such an interaction in Fig. 12. The pathways depicted allow for such an interaction. However, the water–rock ratios of the highest  $\delta D$  samples have the lowest values suggesting a low water–rock ratio. Yet, these are major producing veins, which might be expected to have formed in high permeability, water-dominated systems. Therefore, we prefer to consider that this is a magmatic dominated end-member fluid (see above).

Fluid  $\delta^{18}\text{O}$  and  $\delta D$  data in equilibrium with sericite from the wallrock of Pb–Zn veins and in a temperature range of 210–280°C are shown in Fig. 10b. These fall within and close to the magmatic water box, with little suggestion of significant involvement of other fluids.

Figure 10b also shows the range of calculated fluid  $\delta^{18}\text{O}$  and  $\delta D$  in equilibrium with sericites from high sulfidation alteration in a temperature range of 280–350°C. Whilst two of the five data points plot in the magmatic water box, three of the samples depict a trajectory towards higher  $\delta D$  values. We reject mixing with meteoric fluids because water/rock

**Fig. 12** Plot of water/rock ratio calculations for final water isotope compositions using possible volcanic rock and starting meteoric water compositions and possible extreme ranges of water/rock ratios. Following the method of Field and Fifiarek (1985), the proxy equation for hydrogen isotope composition of the rock used was that for chlorite–water fractionation from Graham et al. (1984) and that for the O isotope calculation for feldspar–water is from Matsuhisa et al. (1979)



ratios are small at around 0.01 to 0.001 and would be unlikely to yield intensely and pervasively altered bodies of rock. The trend towards higher  $\delta D$  values may reflect the poor constraint on the sericite fractionation equation (Suzuoki and Epstein 1976; Sheppard and Gilg 1996; Ojala et al. 1995; Vennemann and O'Neil 1996) or it may be due to the involvement of volcanic gasses (Fig. 12). We favour an essentially magmatic origin for these fluids. The large input of magmatic water for this paragenesis is consistent with its position overlying the monzonite magma chamber.

Fluids in equilibrium with four investigated high sulfidation kaolinite samples in a temperature range of 280–350°C indicate the predominance of magmatic water involved in their deposition (Fig. 10c).

Fluids in equilibrium with the high sulfidation alunite samples were calculated for a temperature range of 280–350°C (Fig. 10d). These data lie at the edge of the magmatic water box in a similar position to high sulfidation sericite; thus, a similar magmatic fluid dominance is suspected.

In Fig. 10d, the calculated fluid  $\delta^{18}\text{O}$  values for barite from the Pb–Zn veins at temperatures between 210 and 280°C (based on mean  $\pm 1\sigma$  for quartz veins with galena and sphalerite) together with the directly measured fluid inclusion  $\delta D$  values are plotted. The data plot right in the quartz-precipitating fluid field and suggest a similar meteoric–magmatic origin for the barite-precipitating fluids. These fluids have no indication of a sea water influence.

Overall, we conclude that magmatic fluids dominated the higher temperature–high sulfidation association, whereas the fluids responsible for the intermediate sulfidation association contained a significant to dominant meteoric water component.

*Model for hydrothermal activity* The model presented in this paper builds upon the one proposed by Marchev and Singer (2002). The geological and geochronological data show that the various phases of hydrothermal activity and mineralization at Madjarovo occurred within a short time period (<310 ka) and were an integral part of the evolution of the Madjarovo volcano. The porphyry style and high sulfidation alteration occurred first and are related to late monzonitic activity. The hydrothermal fluids responsible for the high sulfidation alteration contained a dominant magmatic component that was derived from the main central monzonitic magma chamber. The alteration occurred relatively high in the volcanic edifice and formed a lithocap of which remnants are preserved. The volcano was emergent but the presence of limestones at the base of the volcanic succession indicates that the sea was nearby. Small amounts of meteoric water penetrated the volcano and mixed with the magmatic fluids responsible for alteration (Fig. 3a).

Shortly afterwards, fresh injections of a more differentiated magma into a chamber below the Madjarovo volcano caused uplift and erosion. Differentiation was occurring rapidly in the magma chamber during the eruption of the Upper Unit lavas as evidenced by the progression from basalt to quartz trachyte. The emplacement of the main stage Pb–Zn veins occurred shortly after the last observed igneous event and, during the final stages of differentiation, magmas of a granitic composition may have been formed (Marchev and Singer 2002). The uplift and doming resulted in the opening of further radial fissures. Magmatic fluids initially entered these fissures and were responsible for the wallrock alteration. Later, meteoric waters accessed the fissures and may have mixed with magmatic fluids to create the saline fluids responsible for the Pb–Zn mineralization. We presume that the shoreline had retreated after uplift and that seawater could not enter the magmatic–hydrothermal system (Fig. 3b). The source of the sulphur is not well constrained and igneous, and basement areas should both be considered. However, Pb isotope data on galena and igneous rocks from Madjarovo (Marchev et al. 2005 and references therein) indicate that the lead is derived mostly from the igneous rocks with little input from the local metamorphic basement.

*Comparisons with other porphyry–epithermal systems* Many features of Madjarovo geology suggest that the deposit is essentially a porphyry copper system emplaced in the epithermal environment. These features include the magma composition; early, albeit weak, copper mineralization and alteration; a barren lithocap and late stage base metal mineralization. There are clear similarities between Madjarovo and many gold deposits in the western Pacific where Sillitoe (1989) noted a close spatial and temporal relationship between porphyry stocks and high- and low-sulfidation epithermal gold deposits (in the following discussion, the term low sulfidation is retained as used in the quoted reference, but many, if not all, of these deposits would be reclassified as intermediate sulfidation deposits in the sense of Sillitoe and Hedenquist 2003). Sillitoe (1989) interpreted this as involving early and central acid sulfate alteration dominated by magmatic fluids and later more peripheral adularia–sericite alteration forming in response to the collapse of a meteoric system. The close spatial and temporal association between porphyry and epithermal style alteration seen at Madjarovo is also found in the Lepanto/Far Southeast deposits in the Philippines (Arribas et al. 1995). Here, the intermediate sulfidation Victoria deposit is located alongside the Lepanto high sulfidation copper–gold deposit (Claveria 2001).

Considered in detail, the vertical extent of mineralization, vertical distribution of metals, salinities of ore fluids, and temperatures of mineralization and the Madjarovo Pb–

Zn veins are very similar to the ‘Deep-vein type with boiling’ end member recognised in the Mexican low sulfidation epithermal deposits (Albinson et al. 2001).

The change from intermediate to more felsic magma compositions accompanying changes in the styles of mineralization and alteration is also present in other epithermal deposits (Bonham 1986; McEwan and Rice 1991; Singer and Marchev 2000). Madjarovo is unusual in that all these variations are found in one magmatic–hydrothermal system. In the Spahievo ore field, 40 km west of Madjarovo, Marchev and Singer (1999) and Singer and Marchev (2000) suggested a genetic relationship between the spatially and temporarily associated monzonite porphyry intrusion and high sulfidation alteration on one hand and the rhyolite dykes and a low-sulfidation epithermal gold deposit on the other. The two magmatic–hydrothermal systems are temporarily separated by 500–800 ka and, according to these authors, cannot be driven by a single magmatic body. Limited K–Ar and  $^{40}\text{Ar}/^{39}\text{Ar}$  dating from other areas suggest age differences between the high- and low sulfidation alteration ranging from 300–800 ka in the Plio-Pleistocene Baguio volcano, Philippines, and Tavua Caldera, Fiji (Aoki et al. 1993; Setterfield et al. 1992), up to 1.6 Ma in the Eocene Mount Skukum Au deposit, Yukon Territory, Canada (Love et al. 1998). Thus, the temporal separation between the two hydrothermal systems seen at Madjarovo (<310 ka) is seen to be at the lower end of the spectrum seen elsewhere.

Thermal modelling indicates that small single bodies of magma could sustain hydrothermal activity for a few tens of thousands of years and that a large single body, under exceptional circumstances, for nearly 1 Ma (Cathles et al. 1997). Thus, the Madjarovo hydrothermal activity could be related to the cooling and differentiation of a single body of magma. However, field relationships and the differing isotopic compositions of the fluids involved indicate that they are probably connected to separate magmatic events.

The source of the saline ore fluids for the Pb–Zn veins is an important issue at Madjarovo and for intermediate sulfidation mineralisation elsewhere (Sillitoe and Hedenquist 2003). The fluid inclusion and stable isotope data indicate that the ore fluids were a mixture of meteoric and saline magmatic waters. Considering all of the geological evidence, the most likely scenario is that metalliferous magmatic fluids from an underlying magma chamber entered meteoric-water-filled fractures in a similar way to that proposed for the epithermal base metal veins of the Fresnillo district in Mexico (Simmons et al. 1988). This would have been facilitated not only by the proximal position of the fractures to the volcanic centre but also their radiating aspect that would have enabled magmatic fluids to readily access them. Nevertheless, there is a

greater proportion of meteoric fluid in this later phase of alteration (and mineralization) that would be a natural consequence of increasing permeability (Thompson et al. 1994; Aoki et al. 1993) or increasing depth of magmatic source (Marchev and Singer 2002). At Madjarovo, both factors appear to have been important.

The low copper content of the Madjarovo intermediate sulfidation mineralisation compares with other intermediate sulfidation deposits (Sillitoe and Hedenquist 2003). Copper may be partitioned into the vapour phase during cooling of a magma (Heinrich et al. 1999) and could be lost in a shallow, well-fractured system such as Madjarovo.

Madjarovo is a rare example of a volcanic/sub-volcanic setting where spatial and genetic links between high and intermediate sulfidation (and porphyry) styles of alteration can be demonstrated. In particular, this study suggests that the change from high to intermediate sulfidation systems is largely controlled by the ore fluid composition, i.e. the proportions of magmatic fluid to meteoric fluid, that in turn is controlled by the evolutionary history of the volcanic centre.

*Absence of mineralization associated with high sulfidation alteration* The high sulfidation alteration at Madjarovo is not obviously associated with any mineralization, and removal by erosion can be ruled out as responsible for the absence of mineralization as the palaeosurface was only 150–200 m above the present land surface (Marchev et al. 1997). This situation is not unique, and other examples are known: the Mid-Tertiary Masura Ria volcanic centre; Central Kalimantan, where intermediate sulfidation veins cut a barren lithocap (Thompson et al. 1994); the Plio-Pleistocene Baguio volcano, Philippines (Aoki et al. 1993); and the Eocene Mount Skukum Au deposit, Yukon Territory, Canada (Love et al. 1998). It is perhaps significant that, unlike with other well-known mineralised high sulfidation deposits, e.g. Nansatsu (Hedenquist et al. 1994), vuggy silica is not well developed at Madjarovo within the advanced argillic alteration.

The vuggy silica zone may be important in providing a high permeability zone (fracture permeability) for later-mineralizing fluids (e.g. Stoffregen 1987; White 1991). The failure to develop large amounts of vuggy silica may reflect a relatively small magmatic input to the system and may have been a contributory factor in the system remaining unmineralised. Another possible factor relates to the central position of the alteration that may indicate that it formed at a topographically high level within the volcano and that this restricted the flow of convecting fluids into the advanced argillic alteration zone (Berger and Bonham 1990; Mitchell 1992).

## Conclusions

- At Madjarovo, sulfide sulphur in the main-stage Pb–Zn veins may have been derived by leaching from the metamorphic basement and/or an igneous source. Alternatively, a direct magmatic source is permitted by the oxygen and hydrogen isotope data.
- A combination of  $\delta^{34}\text{S}$ ,  $\delta\text{D}$  and  $\delta^{18}\text{O}$  data show that S in late stage barite from the upper parts of the Pb–Zn veins was probably derived from the disproportionation of  $\text{SO}_2$  in the magmatic system. Local sedimentary sources and seawater sulfate as possible sources of sulphur can be discounted. A similar origin is suggested for the sulphur in alunite from the high sulfidation alteration.
- The stable isotope study of quartz, sericite and kaolinite from the high sulfidation alteration has provided compelling evidence that the fluids had a dominant magmatic component with minor quantities of meteoric water.
- The fluid responsible for the sericitic wallrock alteration of the Pb–Zn veins was essentially magmatic, whereas that responsible for the mineralization was a mixture of meteoric and magmatic waters but certainly containing a significant meteoric component.
- The high and low sulfidation alteration formed from separate fluids and at separate times within the lifetime of the Madjarovo volcano (ca. 600 ka). The former formed above and relatively close to a degassing monzonitic magma in a location where access by meteoric water was limited. The latter formed later and peripheral to the centre of igneous activity in an extensive system of radial fissures that opened in response to resurgent magmatic activity. These were initially invaded by magmatic fluids but meteoric fluids entered the system later, possibly mixed with the magmatic fluids and precipitated the Pb–Zn mineralization.
- Fluids responsible for high and low sulfidation (and porphyry style) alteration and mineralization may all be generated within one relatively short-lived volcanic centre, depending on its magmatic and tectonic evolution. This allows for the possibility of mixing of fluids and the generation of deposits with intermediate characteristics.

**Acknowledgement** We thank Terry Donnelly and Alison MacDonald for the technical support during stable isotope analyses and Barry Fulton for the diagrams. SUERC is funded by Natural Environment Research Council (NERC) and the Scottish Universities Consortium. A.J.B. is funded by the NERC support of the Isotope Community Support Facility at SUERC. We thank Thomas Wagner of Tübingen University for the discussions and for allowing the use of his program for calculating O isotope trajectories resulting from boiling, cooling and mixing. We gratefully acknowledge the constructive reviews of Andrew Campbell and Jon Naden.

## References

- Albinson T, Norman DI, Cole C, Chomiak B (2001) Controls on formation of low-sulfidation epithermal deposits in Mexico: constraints from fluid inclusion and stable isotope data. *Society of Economic Geologists Special Publication* 8:1–32
- Aoki M, Comsti EC, Lazo FB, Matsuhisa Y (1993) Advanced argillic alteration and geochemistry of alunite in an evolving hydrothermal system at Baguio, Northern Luzon, Philippines. *Res Geol* 43 (3):155–164
- Arnaudova R, Velinov I, Gorova M, Arnaudov V, Bonev I, Batandjiev I, Marchev P (1991) Geochemistry of quartz-adularia metasomatites from the Madjarovo tertiary polymetal Au–Ag deposits the East Rhodopes. In: Mrna F (ed) *Exploration geochemistry, 1990. Proceedings of the third international joint symposium of the IAGC and the AGC, Prague*, pp 13–16
- Arribas A, Hedenquist JW, Tetsumaru I, Toshinori O, Concepcion RA, Garcia JS (1995) Contemporaneous formation of adjacent porphyry and epithermal Cu–Au deposits over 300 ka in northern Luzon, Philippines. *Geology* 23:337–340
- Atanasov A (1959) The structure of the lead zinc ore district of Madjarovo. *Annuaire de l'Universite de Sofia Geologie* 52 (2):313–348
- Atanasov A (1962) Mineralization stages, primary zoning and genesis of the complex ore-deposit of Madjarovo. *Annuaire de l'Université de Sofia Géologie* 55(2):229–267
- Berger B, Bonham H (1990) Epithermal gold silver deposits in the western United States: time-space products of evolving plutonic, volcanic and tectonic environments. *J Geochem Explor* 36:103–142
- Berger BR, Eimon P (1983) Conceptual models of epithermal precious metal deposits. In: Shanks WC III (ed) *Volume on unconventional mineral deposits: society of mining engineers. American Institute of Mining Engineering*, pp 191–205
- Bodnar RJ, Reynolds TJ, Kuehn CA (1985) Fluid-inclusion systematics in epithermal systems. In: Berger BR, Bethke PM (eds) *Geology and geochemistry of epithermal systems: society of economic geologists. Rev Econ Geol* 2:73–97
- Bonham HF Jr (1986) Models for volcanic-hosted epithermal precious metal deposits: a review. In: *International volcanological congress, symposium 5, Hamilton, New Zealand, 1986. Proceedings of the University of Auckland Centre for Continuing Education*, pp 13–17
- Breskovska V, Tarkian M (1993) Mineralogy and fluid inclusion study of polymetallic veins in the Madjarovo ore field, Eastern Rhodopes, Bulgaria. *Min Pet* 49:103–118
- Breskovska V, Iliev Z, Mavroudchiev B, Vaptzarov I, Velinov I, Nozharov P (1976) The Madjarovo ore field. *Geochem Miner Petrol* 5:23–57
- Buchanan LJ (1981) Precious metal deposits associated with volcanic environments in the southwest. In: Dickson WR, Payne WD (eds) *Relations of tectonics to ore deposits in the Southwest Cordillera, Arizona. Geol Soc Digest* 14:237–262
- Burg JP, Ivanov Z, Ricou LE, Dimor D, Klain L (1990) Implications of shear-sense criteria for the tectonic evolution of the central Rhodope massif, Bulgaria. *Geology* 18:451–454
- Canfield D, Raiswell R, Wesrich J, Reaves C, Berner R (1986) The use of chromium reduction in the analyses of reduced inorganic sulphur in sediment and shales. *Chem Geol* 54:149–155
- Carrigan C, Mukasa S, Haydoutov I, Kolcheva K (2003) Ion microprobe U–Pb zircon ages of pre-Alpine rocks in the Balkan, Sredna Gora, and Rhodope terranes of Bulgaria: constraints on neoproterozoic and variscan tectonic evolution. *J Czech Geol Soc* 48(1–2):32–33
- Cathles LM, Erendi AHJ, Barrie T (1997) How long can a hydrothermal system be sustained by a single intrusive event? *Econ Geol* 92:766–771

- Claveria RJR (2001) Mineral paragenesis of the Lepanto copper and gold and the Victoria gold deposits, Mankayan mineral district, Philippines. *Res Geol* 51:97–106
- Claypool G, Holser WT, Kaplan IR, Sakai H, Zak I (1980) The age of sulphur and oxygen isotopes in marine sulphate and their mutual interpretation. *Chem Geol* 28:199–260
- Clayton R, Mayeda T (1963) The use of bromine pentafluoride in the extraction of oxygen from oxides and silicates for isotopic analysis. *Geochim Cosmochim Acta* 27:43–52
- Coleman M, Moore M (1978) Direct reduction of sulphates to sulphur dioxide for isotopic analysis. *Anal Chem* 50:1594–1595
- Conrad ME, Petersen U, O'Neil JR (1992) Evolution of an Au–Ag producing hydrothermal system: the Tayoltita mine, Durango, Mexico. *Econ Geol* 87:1451–1474
- Cooke DR, McPhail DC (2001) Epithermal Au–Ag–Te mineralization, Acupan, Baguio district, Philippines: numerical simulations of mineral deposition. *Econ Geol* 96:109–131
- Einaudi MT, Hedenquist JW, Inan EE (2003) Sulfidation state of fluids in active and extinct hydrothermal systems: transitions from porphyry to epithermal environments. *Society of Economic Geologists* 10:285–313
- Fallick AE, Jocelyn J, Hamilton PJ (1987) Oxygen and hydrogen stable isotope systematics in Brazilian agates. In: Rodriguez-Clemente R, Tardy Y (eds) *Geochemistry and mineral formation in the earth surface*. CSIC Madrid and CNRS Paris, pp 99–117
- Field CW, Fifarek RH (1985) Light stable-isotope systematics in the epithermal environment. In: *Geology and Geochemistry of Epithermal Systems*. Reviews in Economic Geology 2:99–128
- Gergelchev VN (1974) Main features and formation stages of the Madjarovo cauldron subsidence and structural conditions for its ore-bearing properties. *Bulletin of the Geological Institute Series of Metal and Nonmetal Mineral Deposits* 23:5–29
- Gilg HA, Sheppard SMF (1996) Hydrogen isotope fractionation between kaolinite and water revisited. *Geochim Cosmochim Acta* 60:529–533
- Godfrey J (1962) The deuterium content of hydrous minerals for the East Central Sierra Nevada and Yosemite National Park. *Geochim Cosmochim Acta* 26:1215–1245
- Goranov A, Atanasov G (1989) Lithostratigraphic subdivision of the East Rhodope and Upper Thracian Palaeogene. *Geol Rhodop* 1:14–21
- Graham CM, Atkinson J, Harmon RS (1984) Hydrogen isotope fractionation in the system chlorite–water. NERC 6th progress report of research, 1981–1984. NERC Publication 25(D):139
- Haas JL Jr (1971) The effect of salinity on the maximum thermal gradient of a hydrothermal system at hydrostatic pressure. *Econ Geol* 66:940–946
- Hall AJ, Boyce AJ, Fallick AE, Hamilton PJ (1991) Isotopic evidence of the depositional environment of Late Proterozoic stratiform barite mineralization, Aberfeldy, Scotland. *Chem Geol* 87:99–114
- Hardy R, Tucker M (1988) X-ray powder diffraction of sediments. In: Tucker M (ed) *Techniques in Sedimentology*. Blackwell, Oxford, p 394
- Harkovska A, Yanev Y, Marchev P (1989) General features of the Palaeocene orogenic magmatism in Bulgaria. *Geol Balcan* 19:37–72
- Haydoutov I, Kolcheva K, Daieva L, Savov I (2001) Island–arc origin of the variegated formations from the east Rhodopes (Avren synform and Bela Reka antiform), Bulgaria. Abstracts. Joint meeting of Europrobe TESZ, TIMPEBAR, Uralides and SW–Iberia projects, 30 September–2 October 2001, Middle East Technical University, Ankara–Turkey, pp 31–32
- Hedenquist JW, Henley R (1985) The importance of CO<sub>2</sub> on freezing point measurements of fluid inclusions from active geothermal systems and implications for epithermal ore deposition. *Econ Geol* 80:1379–1406
- Hedenquist JW, Izawa E, White NC, Giggenbach WF, Saoki M (1994) Geology, geochemistry and origin of high sulfidation Cu–Au mineralization in the Nansatsu district. *Japan Econ Geol* 89:1–30
- Hedenquist JW, Izawa E, Arribas A, White NC (1996) Epithermal gold deposits: styles, characteristics, and exploration. *Resource Geology* 1:17
- Heinrich CA, Gunther D, Audetat A, Ulrich T, Frischknecht R (1999) Metal fractionation between magmatic brine and vapour, determined by microanalysis of fluid inclusions. *Geology* 27:755–759
- Iosifov D, Tsvetkova D, Pchelarov V, Revyakin P, Gergelchev V, Tsvetkov A (1987) Deep structure of Avren–Madjarovo ore zone. Review of the Bulgarian Geological Society 48(2):73–86
- Ivanov R (1960) Magmatism in the East Rhodope Paleogene depression, part I. *Travaux sur la Geologie de Bulgarie. Serie de Geochimie et des Gites Metalliferes et Non-Metalliferes* 1:311–387
- Ivanov Z (1989) Structure and tectonic evolution of the central parts of the Rhodope massif. Guide to excursion E3, CBGA–XIV congress, p 126
- Jaranov D (1960) Tectonics of Bulgaria. Technica, Sofia, p 283
- Jones CE, Tarney J, Baker JH, Gerouki F (1992) Tertiary granitoids of Rhodope, northern Greece: magmatism related to extensional collapse of the Hellenic Orogen? *Tectonophysics* 210:295–314
- Kharkovska A (1984) Tertiary magmotectonic zones in Southwest Bulgaria. In: *Magmatism of the molasse-forming epoch and its relation to endogenous mineralization*. GÚDŠ, Bratislava, pp 9–34
- Kilias SP, Naden J, Cheliotis I, Shepherd TJ, Constandinidou H, Crossing J, Simos I (2001) Epithermal gold mineralisation in the active Aegean volcanic arc: the Profitas Ilias deposit, Milos Island, Greece. *Mineralium Deposita* 36:32–44
- Kockel F, Mollat H, Walther HW (1977) Erläuterungen zur Geologisch-ethnographischen Karte der Chalkidhiki und angrenzender Gebiete 1:100,000 (Nord–Griechenland)–Bundesanstalt für Geowissenschaften und Rohstoffe, Hanover, p 119
- Kolcheva K, Eskenazy G (1988) Geochemistry of metaeclogites from the central and eastern Rhodope Mts (Bulgaria). *Geol Balcan* 18:61–78
- Kozhoukharov D, Kozhoukharova E, Papanikolaou D (1988) Precambrian in the Rhodope massif. In: Zoubek V (ed) *Precambrian in younger fold belts*. Chichester, pp 723–778
- Kozhoukharova E (1984) Origin and structural position of the serpentinized ultrabasic rocks of the Precambrian ophiolitic association in the Rhodope Massif. In: *Geologic position and composition of ophiolite association*. *Geol Balc* 14:9–36
- Love DA, Clark AN, Hodgson CJ, Mortensen JK, Archibald DA, Farrar E (1998) The timing of adularia–sericite-type mineralization and alunite–kaolinite-type alteration, Mount Skukum epithermal gold deposit, Yukon Territory, Canada: <sup>40</sup>Ar–<sup>39</sup>Ar and U–Pb geochronology. *Econ Geol* 93:437–462
- Marchev P, Rogers G (1998) New Rb–Sr data on the bottom and top of the Madjarevo volcano: inferences for the age and genesis of the lavas. *Geochim Miner Petrol* 34:91–96
- Marchev P, Shanov S (1991) Potassium and silica variations in the Palaeogenic Macedonian–Rhodopean–North Aegean volcanic belt: geodynamic and petrogenetic implications. *Geol Balc* 21:3–1
- Marchev P, Singer B (1999) Timing of magmatism, alteration–mineralization, and caldera evolution in the Spahievo ore field, Bulgaria from laser–fusion <sup>40</sup>Ar/<sup>39</sup>Ar dating. In: CJ Stanley et al (ed) *Mineral deposits: processes to processing*. Proceedings of the 5th biennial SGA meeting, London, England, 22–25 August 1999, pp 1271–1274
- Marchev P, Singer B (2002) <sup>40</sup>Ar/<sup>39</sup>Ar geochronology of magmatism and hydrothermal activity of the Madjarovo base-precious metal ore district, eastern Rhodopes, Bulgaria In: Blundell DJ, Neubauer F and von Quadt A (ed) *The timing and location of*

- major ore deposits in an evolving orogen. *Geol Soc (Lond)* 204:137–150
- Marchev P, Iliev Z, Nokov S (1989) Oligocene volcano “Madjarovo.” Guidebook of scientific excursion E–2 (CBGA, XIV congress, Sofia). Alpine magmatism and related metallogeny in Srednogie and Eastern Rhodopes, pp 97–103
- Marchev P, Larson P, Rogers G, Vaselli O, Raicheva R (1994a) Crustal thickness control on the Sr, Nd and O isotopic variation in the Macedonian–Rhodope–North Aegean magmatic belt (MRNAMB). International volcanol congress (IAVCEI), Ankara
- Marchev P, Raicheva R, Larson P (1994b) Magma mixing in a collisional setting: preliminary data from the tertiary volcanism in the Eastern Rhodope mountains, Bulgaria. *Comptes Rendus de l’Academy Bulgare des Sciences* 47(3):63–66
- Marchev P, Nokov S, McCoyd R, Jelev D (1997) Alteration processes and mineralizations in the Madjarovo ore field—a brief review and new data. *Geochem Miner Petrol* 32:47–58
- Marchev P, Raicheva R, Singer B, Downes H, Amov B, Moritz R (2000) Isotopic evidence for the origin of Paleogene magmatism and epithermal ore deposits of the Rhodope Massif. ABCD–GEODE 2000 Workshop, Borovets, Bulgaria, May 2000, p 47
- Marchev P, Downes H, Thirlwall MF, Moritz R (2002) Small-scale variations of  $^{87}\text{Sr}/^{86}\text{Sr}$  isotope composition of barite in the Madjarovo low-sulfidation epithermal system, SE Bulgaria: implications for sources of Sr, fluid fluxes and pathways of the ore-forming fluids. *Miner Depos* 37:669–677
- Marchev P, Raicheva R, Downes H, Vaselli O, Chiaradia M, Moritz R (2004) Compositional diversity of Eocene–Oligocene basaltic magmatism in the eastern Rhodopes, SE Bulgaria: implications for genesis and tectonic setting. *Tectonophysics* 393:301–328
- Marchev P, Kaiser-Rohrmeier M, Heinrich C, Ovtcharova M, von Quadt A, Raicheva R (2005) Hydrothermal ore deposits related to post-orogenic extensional magmatism and core complex formation: the Rhodope Massif of Bulgaria and Greece. *Ore Geol Rev* 27:53–89
- Matsuhisa Y, Goldsmith JR, Clayton RN (1979) Oxygen isotope fractionation in the system quartz–albite–anorthite–water. *Geochim Cosmochim Acta* 43:1131–1140
- Mavroudchiev B (1959) Upper Oligocene intrusions from the Madjarovo ore district. *Annuaire de l’Université de Sofia Géologie* 52(2):251–300
- Maznikov Z, Văleva G (1986) Nouvelles données sur la structure du volcan de Madjarovo. Yearbook of the committee of geology 26:29–38
- McEwan CJA, Rice CM (1991) Trace-element geochemistry and alteration facies associated with epithermal gold–silver mineralization in an evolving volcanic centre, Rosita Hills, Colorado, USA. *Trans Inst Min Metall* 100:B19–B27
- Milev V, Stanev V, Ivanov V (1996) Mining production in Bulgaria, 1878–1995, statistical reference book. Zemina-93 Press, p 196
- Mitchell A (1992) Andesitic arcs, epithermal gold and porphyry-type mineralization in the western Pacific and Eastern Europe. *Trans Inst Min Metall* 101(B):B125–B138
- Mposkos E, Krohe A (2000) Petrological and structural evolution of continental high pressure (HP) metamorphic rocks in the Alpine Rhodope domain (N. Greece). In: Panayides I, Xenopontos C, Malpas J (eds) Proceedings of the 3rd international conference on the geology of the eastern Mediterranean (Nicosia, Cyprus). Geological Survey, Nicosia, Cyprus, pp 221–232
- Naden J, Kiliyas SP, Leng MJ, Cheliotis I, Shepherd TJ (2003) Do fluid inclusions preserve  $\delta^{18}\text{O}$  values of hydrothermal fluids in epithermal systems over geological time? Evidence from paleo- and modern geothermal systems, Milos Island, Aegean Sea. *Chem Geol* 197:143–159
- Ohmoto H, Rye RO (1979) Isotopes of sulfur and carbon. In: Barnes HL (ed) *Geochemistry of hydrothermal ore deposits*. Wiley, New York, pp 509–567
- Ojala VJ, Groves DI, Ridley JR (1995) Hydrogen fractionation factors between hydrous minerals and ore fluids at low temperatures: evidence from the Granny Smith gold deposit. *Miner Depos* 30:328–331
- Peytcheva I, von Quadt A (1995) U–Pb zircon dating of metagranites from Byala-reka region in the eastern Rhodopes. Proceedings of the XV congress of CBGA. *Geol Soc Greece* 4:637–642
- Pflumio C, Boulegue J, Liakopoulos A, Briquieu L (1991) Oxygen, hydrogen, strontium isotopes and metals in the present-day and past geothermal systems of Milos Island (Aegean arc). In: Pagel M, Leroy JL (eds) *Source, transport and deposition of metals*. Balkema, Rotterdam, pp 107–112
- Radonova T (1960) Studies on the mineral composition and alterations of Madjarovo base-metal ore deposit in the eastern Rhodopes. *Travaux Geol Bulg* 1:115–197
- Reyes A (1990) Petrology of Philippine geothermal systems and the application of alteration mineralogy to their assessment. *J Volcanol Geotherm Res* 43:279–309
- Robinson BW, Kusakabe M (1975) Quantitative preparation of  $\text{SO}_2$  for  $^{34}\text{S}/^{32}\text{S}$  analysis from sulfides by combustion with cuprous oxide. *Anal Chem* 47:1179–1181
- Roedder E (1984) Fluid inclusions: Mineralogical Society of America. *Rev Min* 12:644
- Rye RO (1974) A comparison of sphalerite–galena sulfur isotope temperatures with filling temperatures of fluid inclusions. *Econ Geol* 69:26–32
- Rye RO (1993) The evolution of magmatic fluids in the epithermal environment: the stable isotope perspective. *Econ Geol* 88:733–753
- Rye RO, Bethke PM, Wasserman MD (1992) The stable isotope geochemistry of acid sulfate alteration. *Econ Geol* 87:225–262
- Scott A-M, Watanabe Y (1998) ‘Extreme boiling’ model for variable salinity of the Hokko low-sulphidation epithermal gold prospect, south-western Hokkaido, Japan. *Miner Depos* 33:568–578
- Setterfield TH, Mussett AE, Oglethorpe RDJ (1992) Magmatism and associated hydrothermal activity during the evolution of the Tavua Caldera:  $^{40}\text{Ar}/^{39}\text{Ar}$  dating of the volcanic, intrusive and hydrothermal events. *Econ Geol* 87:1130–1140
- Sheppard SMF (1986) Characterisation and isotopic variations in natural waters. In: Valley JW, Taylor HP Jr, O’Neill JR (ed) *Stable isotopes in high temperature geological processes*. Mineralogical Association America. *Rev Min* 16:165–184
- Sheppard SMF, Gilg HA (1996) Stable isotope geochemistry of clay minerals. *Clay Miner* 31:1–24
- Sillitoe RH (1989) Gold deposits in western Pacific island arcs: the magmatic connection. In: Keays RR, Ramsay WRH, Groves DI (eds) *The geology of gold deposits: the perspective in 1988*. *Econ Geol Monogr* 6:274–291
- Sillitoe RH, Hedenquist JW (2003) Linkages between volcanotectonic settings, ore fluid compositions, and epithermal precious metal deposits. *Soc Econ Geol* 10:315–343
- Sillitoe RH, Steele GB, Thompson JFH, Lang JR (1998) Advanced argillic lithocaps in the Bolivian tin–silver belt. *Miner Depos* 33:539–546
- Simmons SF, Browne PRL (1997) Saline fluid inclusions in sphalerite from the Broadlands–Ohaaki geothermal system: a coincidental trapping of fluids being boiled toward dryness. *Econ Geol* 92:485–489
- Simmons SF, Gemmel JB, Sawkins FJ (1988) The Santo Nino silver–lead–zinc veins, Fresnillo district, Zacatecas, Mexico, part 2. Physical and chemical nature of ore-forming fluids. *Econ Geol* 83:1619–1641

- Singer B, Marchev P (2000) Temporal evolution of arc magmatism and hydrothermal activity, including epithermal gold veins, at Borovitsa caldera, southern Bulgaria. *Econ Geol* 95:1155–1164
- Stoffregen R (1987) Genesis of acid-sulphate alteration and Au–Cu–Ag mineralization at Summitville, Colorado. *Econ Geol* 82:1575–1591
- Stoffregen R, Alpers C (1987) Woodhousite and svanbergite in hydrothermal ore deposits: products of apatite destruction during advanced argillic alteration. *Can Min* 25:201–211
- Stoyanov R (1979) Metallogeny of the Rhodope Central Massif. Nedra, Moscow, p 180
- Suzuoki T, Epstein S (1976) Hydrogen isotope fractionation between OH-bearing minerals and water. *Geochim Cosmochim Acta* 40:1229–1240
- Thompson JFH, Abidin NZ, Both RA, Martosuroyo S, Rafferty WJ, Thompson AJB (1994) Alteration and epithermal mineralization in the Masura Ria volcanic center, Central Kalimantan, Indonesia. *J Geochem Explor* 50:429–456
- Velinov I, Nokov S (1991) Main types and metallogenic significance of the Madjarovo hydrothermally altered Oligocene volcanics. *Comptes rendus de l'Academy bulgare des Science* 44(9):65–68
- Vennemann TW, O'Neil JR (1996) Hydrogen isotope exchange reactions between hydrous minerals and molecular hydrogen, 1. A new approach for the determination of hydrogen isotope fractionation at moderate temperatures. *Geochem Cosmochim Acta* 60:2437–2451
- Wagner T, Williams-Jones AE, Boyce AJ (2005) Stable isotope-based modelling of the origin and genesis of an unusual Au–Ag–Sn–W epithermal system at Cirotan Indonesia. *Chem Geol* 219:237–260
- Wasserman M, Rye RO, Bethke PM, Arribas A (1992) Methods for separation and total stable isotope analysis of alunite. US Geological Survey Open-File Report 92–9
- White NC (1991) High sulphidation epithermal gold deposits: characteristics and model for their origin. Geological Survey of Japan, report no. 277, pp 9–20